MEFV genotype of Japanese patients with FMF seem to be different from those of Mediterranean patients, and our survey suggests that there will be a large number of FMF patients even in Japan.

REFERENCES

1. Sohar E, Gafni J, Pras M, Heller H. Familial Mediterranean fever. A survey of 470 cases and review of the literature. Am J Med 1967;43:227-53.
2. Onen F. Familial Mediterranean fever. Rheumatol Int 2006;26:489-96.
3. Ben-Chetrit E, Levy M. Familial Mediterranean fever. Lancet 1998;351:659-64.
4. French FMF Consortium. A candidate gene for familial Mediterranean fever. Nat Genet 1997;17:25-31.
5. The International FMF Consortium. Ancient missense mutations in a new member of the RoRet gene family are likely to cause familial Mediterranean fever. The International FMF Consortium. Cell 1997;90:797-807.
6. Touitou I. The spectrum of familial Mediterranean fever mutations. Eur J Hum Genet 2001;9:473-83.
7. Drenth JP, van der Meer JW. Hereditary periodic fever. N Engl J Med 2001;345:1748-57.
8. Hayashi A, Suzuki T, Shimizu A, Yamamura Y. Periodic fever suppressed by reserpine [letter]. Lancet 1976;13:592.
9. Shinozaki K, Agematsu K, Yasui K, et al. Familial Mediterranean fever in 2 Japanese families. J Rheumatol 2002;29:1324-5.
10. Tomiyama N, Oshiro S, Higashiuesato Y, et al. End-stage renal disease associated with familial Mediterranean fever. Intern Med 2002;41:221-4.
11. Livneh A, Langevitz P, Zemer D, et al. Criteria for the diagnosis of familial Mediterranean fever. Arthritis Rheum 1997;40:1879-85.
12. Nakamura A, Yazaki M, Tokuda T, Hattori T, Ikeda S. A Japanese patient with familial Mediterranean fever associated with compound heterozygosity for pyrin variant E148Q/M694I. Intern Med 2005;44:261-5.
13. Nakamura A, Matsuda M, Tazawa K, Shimojima Y, Ikeda S. Successful treatment with infliximab and low-dose methotrexate in a Japanese patient with familial Mediterranean fever. Intern Med 2007;46:1247-9.
14. Suzuki T, Nakamura A, Yazaki M, Ikeda S. A Japanese case of familial Mediterranean fever with homozygosity for the pyrin E148Q mutation. Intern Med 2005;44:765-6.
15. Matsuda M, Nakamura A, Tsuchiya S, Yoshida T, Horie S, Ikeda S. Coexistence of familial Mediterranean fever and Behçet's disease in a Japanese patient. Intern Med 2006;45:799-800.
16. Timmann C, Muntau B, Kuhne K, Gelhaus A, Horstmann RD. Two novel mutations R653H and E230K in the Mediterranean fever gene associated with disease. Mutat Res 2001;479:235-9.
17. Medlej-Hashim M, Rawashdeh M, Chouery E, et al. Genetic screening of fourteen mutations in Jordanian familial Mediterranean fever patients. Hum Mutat 2000;15:384.
18. Toita N, Hatano N, Kawamura N, Aruga T. Sibling cases of familial Mediterranean fever [abstract] [Japanese]. J Clin Pediatrics (Sapporo) 2007;55:44.
19. Tomiyama N, Higashiuesato Y, Oda T, et al. *MEFV* mutation analysis of familial Mediterranean fever in Japan. Clin Exp Rheumatol 2008;26:13-7.
20. Komatsu M, Takahashi T, Uemura N, Takada G. Familial Mediterranean fever medicated with an herbal medicine in Japan. Pediatr Int 2004;46:81-4.
21. Kim S, Ikusaka M, Mikasa G, et al. Clinical study of 7 cases of familial Mediterranean fever with *MEFV* gene mutation. Intern Med 2007;46:221-5.
22. Sugiura T, Kawaguchi Y, Fujikawa S, et al. Familial Mediterranean fever in three Japanese patients, and a comparison of the frequency of *MEFV* gene mutations in Japanese and Mediterranean populations. Mod Rheumatol 2008;18:57-9.
23. Kataoka H, Kumagai H, Hanai H. Treating familial Mediterranean fever with prazosin hydrochloride. Ann Intern Med 1998;129:424.
24. Yoshida K, Kanaoka S, Kajimura M, et al. A Japanese case of familial Mediterranean fever with family history demonstrating a mutation in *MEFV*. Intern Med 2003;42:761-4.
25. Kotone-Miyahara Y, Takaori-Kondo A, Fukunaga K, et al. E148Q/M694I mutation in 3 Japanese patients with familial Mediterranean fever. Int J Hematol 2004;79:235-7.
26. Yamane T, Uchiyama K, Hata D, et al. A Japanese case of familial Mediterranean fever with onset in the fifties. Intern Med 2006;45:515-7.
27. Taniguchi H, Hiramatsu K, Inomata M, Izumi S, Abo H. A case of familial Mediterranean fever. Japanese J Intern Med 2005;17:621-6.
28. Tunca M, Akar S, Onen F, et al. Familial Mediterranean fever in Turkey: results of a nationwide multicenter study. Medicine (Baltimore) 2005;84:1-11.
29. Mellinkoff SM, Snodgrass RW, Schwabe AD, Mead JF, Weimer HE, Frankland M. Familial Mediterranean fever. Plasma protein abnormalities, low-fat diet, and possible implications in pathogenesis. Ann Intern Med 1962 56:171-82.
30. Pras E, Livneh A, Balow JE Jr, et al. Clinical differences between North African and Iraqi Jews with familial Mediterranean fever. Am J Med Genet 1998;75:216-9.
31. El-Shanti H, Majeed HA, El-Khateeb M. Familial Mediterranean fever in Arabs. Lancet 2006;367:1016-24.
32. Livneh A, Langevitz P, Yael S, et al. MEFV mutation analysis in patients suffering from amyloidosis of familial Mediterranean fever. Amyloid 1999;6:1-6.
33. Chae JJ, Wood G, Masters SL, et al. The B30.2 domain of pyrin, the familial Mediterranean fever protein, interacts directly with caspase-1 to modulate IL-1 beta production. Proc Natl Acad Sci USA 2006;103:9982-7.
34. Booth DR, Gillmore JD, Lachmann HJ, et al. The genetic basis of autosomal dominant familial Mediterranean fever. QJM 2000;93:217-21.
35. Pasa S, Altintas A, Devecioglu B, et al. Familial Mediterranean fever gene mutations in the Southeastern region of Turkey and their phenotypical features. Amyloid 2008;15:49-53.
36. Tchernitchko D, Legendre M, Cazeneuve C, Delahaye A, Niel F, Amselem S. The E148Q *MEFV* allele is not implicated in the development of familial Mediterranean fever. Hum Mutat 2003;22:339-40.
37. Ozen S, Bakkaloglu A, Yilmaz E, et al. Mutations in the gene for familial Mediterranean fever: do they predispose to inflammation? J Rheumatol 2003;30:2014-8.
38. Aksentijevich I, Torosyan Y, Samuels J, et al. Mutation and haplotype studies of familial Mediterranean fever reveal new ancestral relationships and evidence for a high carrier frequency with reduced penetrance in the Ashkenazi Jewish population. Am J Hum Genet 1999;64:949-62.
39. Ben-Chetrit E, Lerer I, Malamud E, Domingo C, Abeliovich D. The E148Q mutation in the *MEFV* gene: is it a disease-causing mutation or a sequence variant? Hum Mutat 2000;15:385-6.
40. Topaloglu R, Ozaltin F, Yilmaz E, et al. E148Q is a disease-causing *MEFV* mutation: a phenotypic evaluation in patients with familial Mediterranean fever. Ann Rheum Dis 2005;64:750-2.
41. Booth DR, Lachmann HJ, Gillmore JD, Booth SE, Hawkins PN. Prevalence and significance of the familial Mediterranean fever gene mutation encoding pyrin Q148. QJM 2001;94:527-31.
42. Domingo C, Touitou I, Bayou A, et al. Familial Mediterranean fever in the 'Chuetas' of Mallorca: a question of Jewish origin or genetic heterogeneity. Eur J Hum Genet 2000;8:242-6.

Structural basis for the multiple interactions of the MyD88 TIR domain in TLR4 signaling

Hidenori Ohnishi[a], Hidehito Tochio[b,1], Zenichiro Kato[a,c,d,1], Kenji E. Orii[a], Ailian Li[a], Takeshi Kimura[a], Hidekazu Hiroaki[e], Naomi Kondo[a,c,d], and Masahiro Shirakawa[b,f]

[a]Department of Pediatrics, Graduate School of Medicine, [c]Center for Emerging Infectious Diseases, and [d]Center for Advanced Drug Research, Gifu University, Gifu, 501-1194, Japan; [b]Department of Molecular Engineering, Graduate School of Engineering, Kyoto University, Kyoto, 615-8510, Japan; [e]Division of Structural Biology, Graduate School of Medicine, Kobe University, 7-5-1, Kusunoki-cho, Chuo-ku, Kobe, Hyogo, 650-0017, Japan; and [f]Core Research for Evolutional Science and Technology, Japan Science and Technology Corporation, Hon-cho 4-1-8, Kawaguchi, Saitama, 332-0012, Japan

Edited by Jack L. Strominger, Harvard University, Cambridge, MA, and approved April 29, 2009 (received for review December 19, 2008)

Myeloid differentiating factor 88 (MyD88) and MyD88 adaptor-like (Mal) are adaptor molecules critically involved in the Toll-like receptor (TLR) 4 signaling pathway. While Mal has been proposed to serve as a membrane-sorting adaptor, MyD88 mediates signal transduction from activated TLR4 to downstream components. The Toll/Interleukin-1 receptor (TIR) domain of MyD88 is responsible for sorting and signaling via direct or indirect TIR–TIR interactions between Mal and TLR4. However, the molecular mechanisms involved in multiple interactions of the TIR domain remain unclear. The present study describes the solution structure of the MyD88 TIR domain. Reporter gene assays revealed that 3 discrete surface sites in the TIR domain of MyD88 are important for TLR4 signaling. Two of these sites were shown to mediate direct binding to the TIR domain of Mal. Interestingly, Mal-TIR, but not MyD88-TIR, directly binds to the cytosolic TIR domain of TLR4. These observations suggested that the heteromeric assembly of TIR domains of the receptor and adaptors constitutes the initial step of TLR4 intracellular signal transduction.

docking simulation | Mal | innate immunity | NMR | protein structure

Myeloid differentiating factor 88 (MyD88) is a cytosolic adaptor protein that plays essential roles in both innate and acquired immune responses by mediating signal transduction pathways that are initiated by Toll-like receptors (TLRs) and IL-1 and IL-18 receptors (IL-1R and IL-18R). MyD88 consists of an N-terminal death domain (DD) (approximately 90 aa residues), a C-terminal Toll/Interleukin-1 receptor (TIR) domain (approximately 150 aa residues), and a short connecting linker (1). In innate immune responses, the TIR domain of MyD88 has pivotal functions in the formation of signal initiation complexes involving the cytosolic domain of TLRs. The best characterized pathway is the TLR4 pathway, in which the cytosolic TIR domain of LPS-stimulated TLR4 interacts with the TIR domain of MyD88 (MyD88-TIR), in cooperation with another TIR-containing adaptor protein, MyD88 adaptor-like (Mal). Subsequently, signal is transmitted to the IL-1 receptor-associated kinase (IRAK) through an interaction between the death domains of MyD88 and IRAK. This eventually activates the transcription factors NF-κB and activator protein 1 (AP-1) via a phosphorylation cascade (2).

MyD88 has been reported to be involved in signaling pathways initiated by all TLRs thus far reported, with the exception of TLR3 (3). Of the MyD88-dependent pathways involving TLR2, 4, 5, 7, and 9, only the TLR2 and TLR4 pathways require Mal for efficient signal transduction (4). TLR4 also possesses the MyD88-independent signaling pathway, which comprises other TIR-containing cytosolic adaptors, TIR domain-containing adaptor inducing IFN-β (TRIF), TRIF-related adaptor molecule (TRAM), and sterile α and huntingtin-elongation-A subunit-TOR (HEAT) Armadillo motifs (SARM) (5). Therefore, in general, specific complexes involving more than one TIR-containing adaptor are likely to be required for initiation of each TLR signal transduction pathway.

Recently, Kagan and Medzhitov (6) revealed that MyD88 and Mal have distinctly different roles in TLR4 signaling: MyD88 serves as an essential "signaling adaptor," which transmits signals from ligand-activated TLRs to downstream factors to initiate kinase-dependent signaling cascades, while Mal functions as a "sorting adaptor," which recruits MyD88 to the plasma membrane via its PIP2 binding domain to promote interaction between MyD88 and activated TLR4 beneath the membrane. Indeed, Mal was shown to be dispensable for TLR4 signaling when MyD88 is fused to a PIP2 targeting domain. In the TLR4-TRIF pathway, TRAM has been proposed to serve as a sorting adaptor, which delivers TRIF to a specific membrane portion via its myristoylation site (7). These findings suggest that specific combinations of "sorting" and "signaling" TIR-containing adaptors might be involved in TLR signaling pathways.

The specificities of TIR–TIR interactions between adaptors, and between adaptors and TLRs, define the formation of various complexes that initiate TLR signaling pathways. However, little is known about the mechanism of heteromeric interactions between TIR domains. The crystal structures of cytosolic TIR domains of the membranous receptors, TLR1, TLR2, TLR10, and IL-1RAPL have been reported (8–10), and the homomeric TIR interfaces observed in the crystals have been described. However, the functional relevance of these homomeric interactions remains obscure because the formation of a homomeric dimer in these TIR domains has not been observed in solution (9, 10). Based on crystal structures and mutational data, several structural models have been proposed for heteromeric TIR–TIR interactions, which commonly suggest the importance of the so-called BB loop in these interactions (11, 12).

The present study describes the solution structure of MyD88-TIR using NMR spectroscopy. The isolated domain was shown to exist as a monomer in solution state on the basis of size-exclusion chromatography, although full-length MyD88 forms a dimer, which appears to be mediated via homomeric interactions within its death domain. By combining in vitro mutational binding experiments with an NF-κB reporter system in mammalian cells, 2 surface sites were identified as binding interfaces for the TIR domain of the sorting adaptor Mal, one of which includes a critical residue for MyD88 function, whose mutation causes the pyogenic bacterial infections

Author contributions: H.O., H.T., Z.K., N.K., and M.S. designed research; H.O., H.T., Z.K., K.E.O., A.L., T.K., and H.H. performed research; H.O., H.T., Z.K., and M.S. analyzed data; and H.O., H.T., Z.K., and M.S. wrote the paper.

The authors declare no conflict of interest.

This article is a PNAS Direct Submission.

Freely available online through the PNAS open access option.

Data deposition: The atomic coordinates have been deposited in the Protein Data Bank, www.pdb.org (PDB ID code 2Z5V).

[1]To whom correspondence may be addressed. E-mail: tochio@moleng.kyoto-u.ac.jp or zen-k@gifu-u.ac.jp.

This article contains supporting information online at www.pnas.org/cgi/content/full/0812956106/DCSupplemental.

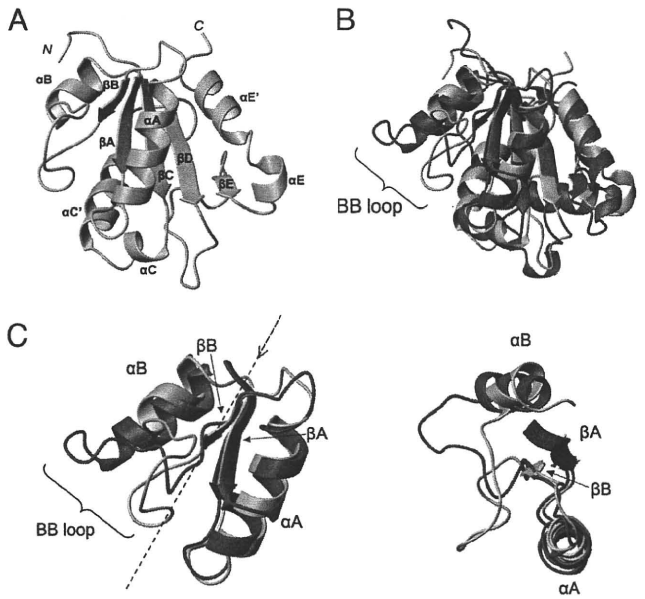

Fig. 1. Solution structure of the TIR domain of human MyD88. (*A*) A representative ribbon drawing of the NMR structure of MyD88, generated with MOLMOL 2K.2. The notation of the secondary structures (βA-βE, αA-αC, and αE) is based on TLR TIR domains. (*B* and *C*) A superimposed representation of MyD88-TIR (sky blue) and the crystal structure of the TIR domain of TLR2 (orange). Although the β-sheet cores are similar (rmsd = 0.90 Å), there are differences in some regions.

(13). Furthermore, the in vitro binding experiments demonstrated that MyD88-TIR does not directly bind to the cytosolic TIR domain of TLR4, while Mal-TIR does. The distal location of the Mal binding sites on the MyD88-TIR surface suggests that the TIR domain of MyD88 simultaneously interacts with 2 Mal-TIR molecules, which may provide a highly efficient scaffold for signal transduction.

Results

Structure Determination of the TIR Domain of MyD88. Based on sequence comparison between TIR domains, a region was selected that comprised residues 148–296 of human MyD88 and was used for structure determination by solution NMR spectroscopy (see Fig. S1). In the buffer used for structural studies, MyD88-TIR resided in a monomeric state, as assumed from size-exclusion chromatography. However, the death domain including internal domain (DD+ID) of MyD88 existed in a dimeric state (see Fig. S2). Therefore, the reported MyD88 dimerization was likely mediated by DD+ID but not by the TIR domain (14). The TIR domain structure of human MyD88 (residues 157–296), which presented the lowest overall energies in the 20 final structures generated by calculations, is shown in Fig. 1*A*. Statistics for the final 20 conformers are summarized in Table S1, which shows that the rmsd for the coordinates of backbone heavy atoms (N, Cα, and C') of residues 157–185, 188–194, and 203–295 is 0.45 Å. The N-terminal 9 residues (148–156) displayed random coil propensity, which was characterized by the lack of medium-to-long range NOESY cross-peaks for the region. Hence, these residues were omitted from the figure and statistics for clarity.

Previous studies have indicated that 3 short, sequence motifs, called box 1–3 motifs, which are (F/Y)DA, RDXXPG, and FW, respectively, are conserved between TIR domains (see Fig. S1) (15). Of these, the box 2 motif, which resides in the so-called BB loop region, has been suggested to be important for TIR–TIR interactions and specificities (8, 16). In the calculated conformers of MyD88-TIR, a section of the BB loop, namely residues 194–208, was not well converged. With the exception of Gly-201, Val-204, and Ser-206, the backbone amide resonances of these residues were not identified in 2D ^{1}H-^{15}N hetero-nuclear single quantum coherence (HSQC) spectra, although resonances of some side chain protons were observed and assigned in HCCH-TOCSY and 3D ^{13}C-edited NOESY spectra. This region appeared to not form a single, definite structure, as judged from observations of a relatively few number of long-range NOEs. A {^{1}H}-^{15}N heteronuclear NOE experiment showed that some main-chain amide groups in the BB loop region, namely Gly-201, Val-204, and Ser-206, displayed NOE values of 0.67, 0.55, and 0.67, respectively, which were less than the average value for residues 157–297 (0.76 ± 0.09). These results implied that the BB loop was mobile in solution. The presumed conformational flexibility in the BB loop region might exert broadening effects due to chemical exchange, which results in absence of the backbone amide resonances of residues 195–200, 202, and 203. In addition, the turn region comprising residues 185–188, which follows helix αA, was poorly defined as the main chain amide resonances of Thr-185, Asp-186, Tyr-187, and Arg-188 could not be identified in the HSQC spectrum.

During the preparation of this manuscript, Rossi et al. released the solution structure of the TIR domain of human MyD88 in the Protein Data Bank (PDB ID: 2JS7). The overall folding was identical to our findings, despite minor differences. However, a detailed comparison of these 2 structures would not be appropriate, because of substantial differences in solution conditions, such as organic additives and pH. The structure of Rossi et al. was determined in a buffer containing 5% acetonitrile at pH 5.0, while the present structure determination was performed in a buffer at pH 6, with no organic solvent.

Structural Description of the TIR Domain of MyD88, and Comparison with Other TIR Domains. The MyD88 TIR domain structure (residues 157–296) comprised a central 5-stranded parallel β-sheet (βA–βE) surrounded by 4 α-helices (αA–αC and αE) (Fig. 1*A*). As predicted, the global fold was similar to what was observed in previously determined crystal structures of TIR domains of receptors TLR1, TLR2, TLR10, and IL-1RAPL (PDB codes: 1FYV, 1FYW, 2J67, and 1T3G, respectively). Of the known structures, the MyD88 TIR domain exhibited highest sequence similarity to TLR2. Fig. 1 *B* and *C* show superimposed representations of the TIR domain structures from MyD88 and TLR2. While the β-sheet cores displayed high structural similarity, as indicated by an rmsd value for backbone N, Cα, and C' of 0.90 Å, several regions displayed notable conformational differences. The largest structural discrepancy was observed in the region from the BB loop (Ser-194-Ala-208 of the MyD88 TIR domain) to αB (Fig. 1*C*). The BB loop was exposed to solvent in MyD88 and TLR2, but the direction in which the loops orient was markedly different. This was mainly due to a structural difference in the C-terminal region of the BB loop (residues 205–208), which precedes αB of MyD88. These residues adopted an extended conformation in MyD88, whereas corresponding residues are involved in an α-helix (αB) in TLR2. Therefore, αB of MyD88 was much shorter than TLR2. Another major conformational difference was the lack of an α-helix in the region between strands βD and βE (residues 257–273) of the MyD88 TIR domain (see Fig. S1). This region adopted an extended and a short helical coil conformation in MyD88, but the corresponding residues formed an α-helix (αD) in TLR2 (positions 266–270 in MyD88 numbering).

Cell-Based Functional Assays of the MyD88 TIR Domain in TLR4 Signaling Pathways. To explore residues that are important for function of the MyD88 TIR domain, we performed mutational analysis of the domain, using dominant negative effects of ectopically expressed isolated TIR domain (17). For the assay, a luciferase reporter system for NF-κB activation was constructed in HEK293 cells, where MyD88-TIR or mutants harboring single amino acid substitutions of surface residues, was ectopically expressed. Expression of

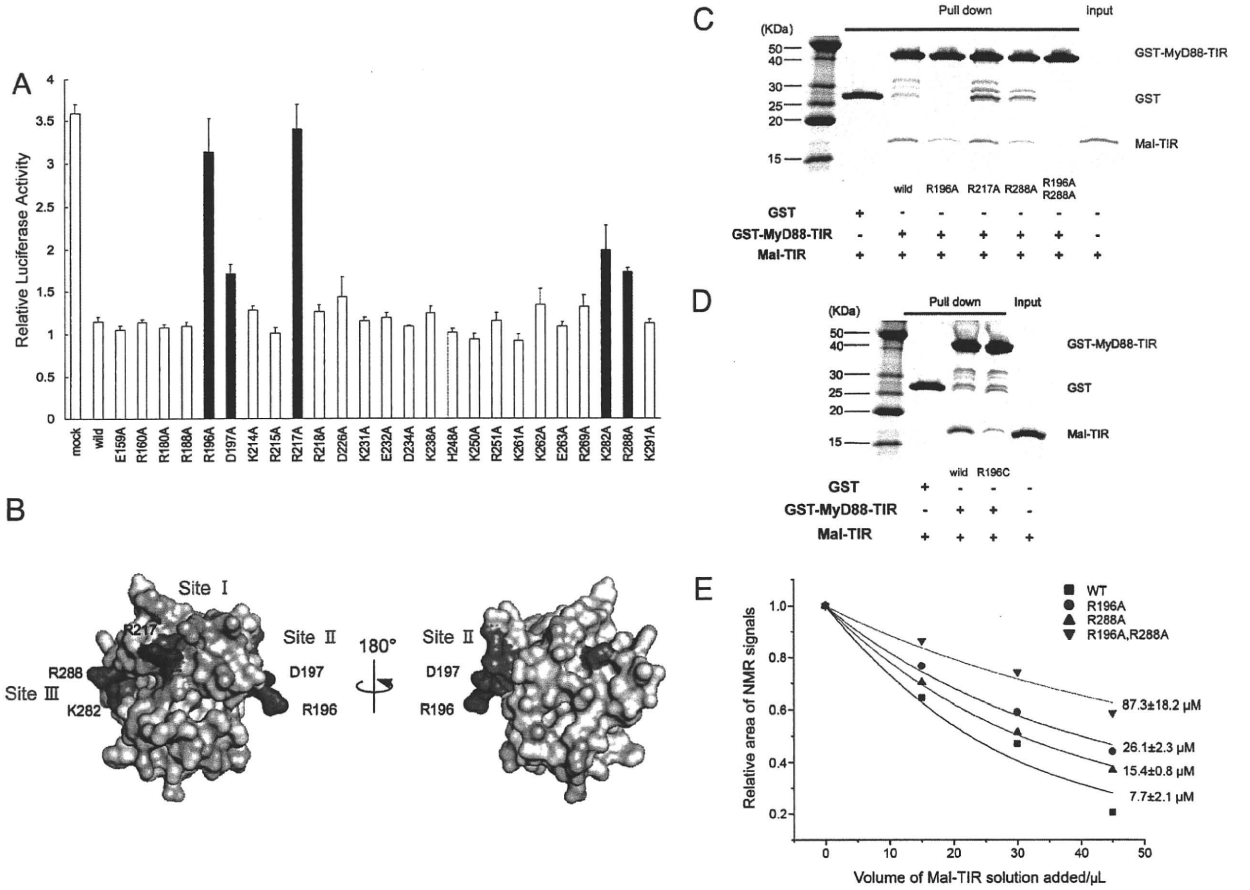

Fig. 2. Functional sites for signaling and binding sites for Mal. (*A*) The NF-κB reporter gene assay of MD2 cotransfected with LPS-induced (1.0 μg/ml) 293-hTLR4A-HA cells. In these graphs, each column indicates relative luciferase activity of stimulated cells over nonstimulated cells. Color code: black bars indicate a significant increased NF-κB activity, compared with the wild-type group. The statistical significance of differences in luciferase activities between wild type and mutants was analyzed using the Dunnett's multiple comparison test. Statistical significance was assumed to be $P < 0.05$. (*B*) Results of the functional assays of LPS/TLR4 signaling presented on the 3D structure of the TIR domain of MyD88. The results of the functional assays are mapped onto the molecular surface of the MyD88 TIR domain. The amino acid residues judged to be significant by the luciferase assay are shown in red, while nonsignificant residues are shown in light brown. The conserved motifs of boxes 1–3 (FDA of box1, VLPG of box2, FW of box3) are shown in blue. (*C*) Assay of binding of Mal TIR domain and MyD88 TIR domain wild type or mutants. Alanine substitutions in Site II (R196A) or Site III (R288A) in MyD88 resulted in reduced interaction with Mal. The double alanine substituted mutant of Site II and Site III caused complete abolition of the interaction with Mal. (*D*) Cysteine substitution in R196 also caused reduced interaction with Mal. (*E*) Plots of relative integrated area of NMR signals, which were derived from NMR titration data, in a function of added volume of Mal-TIR into ^{15}N MyD88-TIR sample. The best-fit lines to the data, assuming a simple 1:1 complex model, are also shown. Apparent dissociation constants calculated are also indicated with standard errors (see Fig. S3). The black box, red circle, blue triangle, and green triangle indicate the dissociation curves of wild-type, R196A, R288A, and R196A-R288A, respectively.

MyD88-TIR, which lacked the N-terminal death domain and thus was supposedly unable to transmit signals, suppressed LPS-induced luciferase expression. This effect was presumably due to inhibition of signaling pathways by competitive binding of the isolated TIR domain to signaling components that interact with endogenous MyD88. When a TIR mutant harboring a substitution of a functionally important residue is expressed, such suppression is alleviated, which leads to higher LPS-induced luciferase activity than observed with a TIR domain harboring the wild-type sequence. It should be noted that the dominant negative effect of ectopically expressed TIR domain has been used for functional analysis of some key residues of MyD88-TIR in IL-1 signaling (11).

Results from luciferase assays of mutant-expressing cells upon LPS stimulation are shown in Fig. 2*A*. LPS addition to HEK293 cells expressing MD2 and TLR4 resulted in an approximately 3-fold increase in reporter activity, which was consistent with a previous report (18). Alanine substitution of 5 residues, Arg-196, Asp-197, Arg-217, Lys-282, or Arg-288 resulted in significantly reduced inhibitory effects in LPS-induced luciferase activity. Interestingly, these 5 residues are closely associated with the box 1, 2, and 3 motifs, which are highly conserved across TIR domains (see Fig. S1). Arg-196 and Asp-197 are located within the box 2 motif. The side chains of Lys-282 and Arg-288 form a continuous protein surface with box 3 forming residues, and Arg-217 is located distant in the sequence, but proximal in space to the box 1 motif (Fig. 2*B*). Hence, we designated the sites that these residues form as Site II, Site III, and Site I, respectively.

Binding Sites of MyD88-TIR for Mal. Because Site I, Site II, and Site III of the MyD88 TIR domain are important for TLR4-mediated cellular responses following LPS stimulation, the involvement of these sites was examined in direct binding to the TIR domain of Mal (Mal-TIR), the sorting adaptor in MyD88-dependent TLR4 pathways (19). The effect of alanine substitution of Arg-196, Arg-217, or Arg-288 (which forms Site II, Site I, and Site III of the MyD88 TIR domain, respectively) on interactions with Mal-TIR was analyzed by GST pull-down assay. Mal-TIR was pulled down by wild-type MyD88-TIR. However, substitution of either Arg-196 or

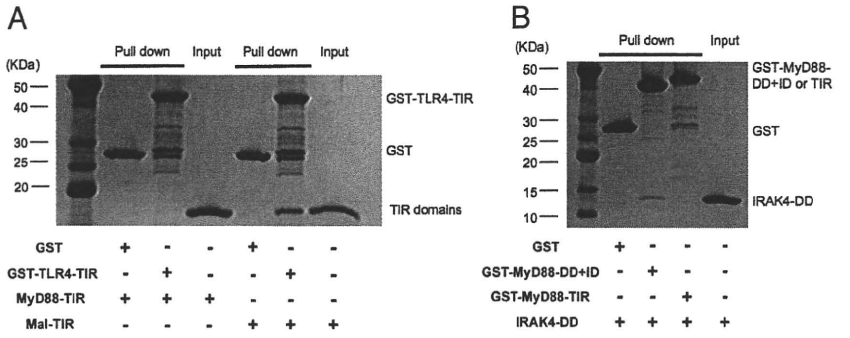

Fig. 3. Direct interactions of MyD88, Mal, TLR4, and IRAK4. (*A*) Binding assay of the TLR4 TIR domain with the MyD88 TIR domain or Mal TIR domain. GST-TLR4-TIR binds Mal-TIR but not MyD88-TIR. (*B*) Binding assay of the IRAK4 death domain with the MyD88 TIR domain or death domain. IRAK4-DD binds the MyD88-DD+ID but not MyD88-TIR.

Arg-288 resulted in moderate, but significant, decreases in MyD88-TIR affinity for Mal-TIR. The MyD88-TIR affinity of the Arg-196 and Arg-288 double-substituted mutant for Mal-TIR was completely abolished (Fig. 2*C*). In contrast, the Arg-217 mutation had no significant effect. The results, therefore, suggested that Site II and Site III, but not Site I, contributed to the interface with Mal-TIR. In addition, Arg-196 substitution by cysteine, which was detected in MyD88 deficiency patients (13), also caused reduced interaction with Mal (Fig. 2*D*). The effect of alanine substitution of those arginine residues on interactions with Mal-TIR was also examined by observing 2D ^{1}H-^{15}N correlation NMR spectra of ^{15}N-labeled MyD88-TIR and its derivative in the absence or presence of various concentrations of nonlabeled Mal-TIR. The ^{15}N-labeled MyD88-TIR signals uniformly decreased upon titration of Mal-TIR (see Fig. S3). Signal attenuation was presumably due to increased apparent molecular weight upon complexation or chemical exchange (Fig. 2*E*). A MyD88-TIR mutation of either Arg-196 or Arg-288 caused moderate effects. However, double mutations of these residues resulted in large effects on signal attenuation, suggesting that signal attenuation was due to interactions between TIR domains of MyD88 and Mal. The apparent dissociation constants were estimated from the signal attenuation of wild-type and mutant MyD88 as previously described (Fig. 2*E*) (20). These results indicated that contributions from Site II and Site III to the interaction were comparable to each other. It should be noted that the effect of tested alanine substitution on the structure of the TIR domain was minor and only limited to the region close to the mutational sites, as judged from the 2D spectra of those mutants. Thus, these substitutions do not affect the opposite functional surface. Therefore, allosteric effect was neglected in interpreting the data.

The Function of Site I in TLR4 Signaling. Site I could serve as an interaction site with cytoplasmic TIR domain of TLR4 (TLR4-TIR), as previously suggested (6). However, an interaction between TIR domains of MyD88 and TLR4 was not detected (Fig. 3*A*). The GST pull-down experiment in the present study further demonstrated that the DD of IRAK4 exhibited no detectable binding activity to MyD88-TIR, but rather bound to MyD88 that lacked the TIR domain (Fig. 3*B*). This indicated that Site I was not involved in interactions with the downstream effector IRAK4, although results from a previous study showed that a small region of TIR, which included box 1 motif, ID, and DD of MyD88, interacts with IRAK4 (21).

Discussion

The TIR domain is typically composed of 135–160 aa residues, with sequence conservation ranging from 20 to 30%. While the hydrophobic core residues are conserved, the surface exposed residues vary greatly between TIR domains. Consequently, the distribution of surface electrostatic potential differs significantly between TIR domains (22), possibly underlying the differences in binding specificity. For TIR domains of membranous receptors, 4 structures from TLR1, TLR2, TLR10, and IL-1RAPL have been reported (8–10). When comparing these, the BB loop of MyD88 displayed the largest structural difference (Fig. 1*C*). The BB loop region has been proposed to be important for interactions between TIR domains. Thus, structural deviation of the BB loop, and differences in surface electrostatic potential, might reflect specificities of TIR–TIR interactions. It should be noted that the isolated MyD88-TIR domain existed as a monomer in solution state, while some TIR domains have been reported to form a dimer in crystal structure (9, 10). On the other hand, full-length MyD88 is known to form a dimer, which seems to be mediated via homomeric interactions between the death domains (see Fig. S2).

The present study identified 3 functional surface sites (Sites I–III) of MyD88-TIR that were important for the LPS-activated TLR4-signaling pathway. Two of these sites, Sites II and III, served as binding sites for Mal-TIR (Fig. 2 *C* and *E*). Results from the GST pull-down and NMR titration experiments suggested that these 2 sites equally contributed to interactions between MyD88-TIR and Mal-TIR. The Site II-forming residues Arg-196 and Asp-197 were located in the BB loop, and were highly conserved across TIR domains (see Fig. S1). Another Mal binding site, Site III, which was formed by 2 basic residues, Lys-282 and Arg-288, flanks the box 3 comprised of FW motif, creating a positively charged surface patch. Because basic amino acids were conserved at positions 282 and 288 (see Fig. S1), this positively charged patch appeared to be common in TIR domains. The present data revealed that Arg-217 in Site I played a crucial role in the TLR4-mediated cellular response to LPS stimulation but was not involved in direct binding to Mal-TIR (Fig. 2*C*). In the GST pull-down experiments, direct interaction of MyD88-TIR with either the TIR domain of TLR4 or the death domain of IRAK4 was not observed (Fig. 3). This was consistent with previous observations that MyD88 does not directly bind to the cytosolic domain of TLR4 (23). Therefore, Site I is unlikely involved in MyD88 interaction with any of the known possible binding partners, such as Mal, TLR4, and IRAK4, but might serve as a contact surface with a yet unidentified MyD88 binding protein or specific membrane portion. The functional role of Site I in TLR4 signaling remains to be clarified in further studies.

The 2 Mal binding sites of MyD88-TIR, Sites II and III, are distantly located from each other and are on opposite molecular surfaces. Thus, it is impossible to assume that one Mal-TIR can make simultaneous contact with both MyD88-TIR sites. In addition, contributions from Site II and Site III to the interaction were shown to be comparable to each other. Thus, assuming 2 Mal-TIR molecules would bind to one MyD88-TIR molecule, we constructed a complex model between MyD88-TIR and Mal-TIR using a molecular docking method similar to previous studies (12, 24). The

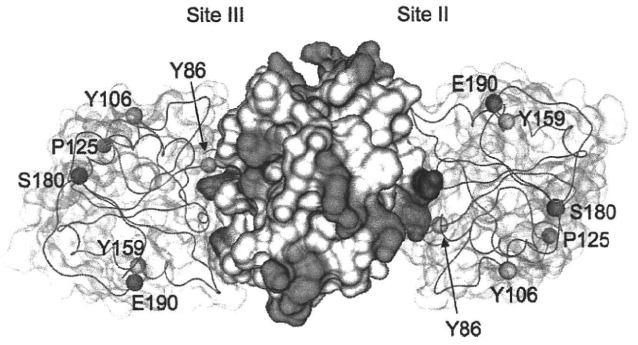

Fig. 4. Structural model of signaling complex formed by MyD88 and Mal. The Mal binding sites, Sites II and III residues, are shown in red, and noncritical residues for signaling and Site I residue are shown in light blue. The positions of the previously reported functional residues (P125, S180, and E190) are shown as orange spheres, and the phosphorylation sites in Mal for signaling, Tyr-86, Tyr 109, and Tyr-159, are shown as yellow spheres.

model indicated that Sites II and III residues are well situated at the interface centers of each Mal-TIR. In addition, all noncritical residues, including Arg-217 (Site I), avoided the interfaces, which supported validity of this model (Fig. 4). Previous reports have shown that P125H mutation or S180L polymorphism of Mal causes decreased interactions between Mal and TLR4 or TLR2, respectively, but has no effect on interactions between Mal and MyD88 (25, 26). Moreover, the TRAF-6 binding site on Mal was shown to include Glu-190 (27). These 3 Mal residues were not included in the Mal-MyD88 complex model interfaces (Fig. 4). Therefore, the model suggested that MyD88-TIR binding might not interfere with interactions between Mal-TIR and TLR4, TLR2, or TRAF-6. Recently, Tyr-86 phosphorylation of Mal was shown to negatively regulate interactions with MyD88 (28). In addition, Tyr-86 mutation, not Tyr-106 or Tyr-159, significantly altered affinity of Mal to MyD88. These observations were consistent with the present complex model, in which Tyr-86, not others, was at the molecular interface (Fig. 4). Moreover, the model predicted that Tyr-86 phosphorylation might perturb MyD88 interface steric complementarity of Mal and result in an electrostatic repulsion to the acidic surface of MyD88-TIR that Mal binds to.

Recently, one of the Site II residues, Arg-196, has just been found to be mutated to cysteine in the new primary immuno-deficiency (MyD88 deficiency) patients (13). This mutation did not cause destabilization of the MyD88 protein, but showed a significant decrease of the direct binding ability between MyD88-TIR and Mal-TIR (Fig. 2*D*). Patients with the MyD88 deficiency were highly susceptible to Gram-positive bacteria, while they showed normal resistance to other kinds of pathogens, such as Gram-negative bacteria and viruses. The phenotypes suggest that TLR2 signaling is more critical than other self-defense systems in early life (3) because the other innate immune signaling pathways have a kind of redundancy, acting as alternative signaling pathways; i.e., TLR2 and TLR4 signaling needs MyD88 and Mal to signal, but TLR4 has other MyD88-independent pathways with TRIF (5). It suggests that the Gram-positive bacterial recognition system is much more dependent on TLR2/MyD88/Mal signaling. The loss of interaction between MyD88 and Mal caused by the mutation would be a critical molecular mechanism for MyD88 deficiency patients.

It is of special interest that the TIR domain of Mal, and not MyD88, directly interacted with the TIR domain of TLR4 (Fig. 3*A*) as described in the previous predicted docking model (29). This observation raises the possibility that Mal-TIR might simultaneously bind to the TIR domains of TLR4 and MyD88, and thereby mediate association as previously predicted (5). Because Mal has been shown to be dispensable for TLR4 signaling when MyD88 is artificially fused to a PIP2 targeting domain (6) there is the possibility that weak interactions between TIR domains of MyD88 and TLR4 mediates signal transduction. Alternatively, an unidentified alternate Mal-independent pathway could contribute to signaling as previously discussed (30). Previous mutation analysis suggests that Mal Pro-125 contributes a binding interface with TLR4 (26). This residue was located distal to the putative MyD88 interface in the present MyD88:Mal complex model and was therefore consistent with the hypothesis that Mal-TIR mediates TIR–TIR interactions between TLR4 and MyD88.

Conclusion

Structure determination combined with functional assays of human MyD88-TIR revealed that 3 sites, which are related to conserved boxes 1–3 of the domain, were important for the LPS/TLR4 pathway. Two of these sites were located at opposite surfaces of the molecule and were shown to mediate direct interaction with Mal-TIR. Thus, the 2 independent binding sites served by MyD88-TIR might contribute to formation of higher order TIR–TIR complexes, which may result in amplification of TLR signal activation. Identification of the key residue in MyD88, which is a direct interacting residue for Mal, is of the clinical significance because one of these residues was shown to be critical for the primary immunodeficiency syndrome. Distribution of the 3 functional sites dispersed on the molecular surface of MyD88-TIR suggested that MyD88 provided multiple interaction surfaces to protein factors that form the signal initiation complex at the cytosolic TLR4 domain. Knowledge of the sites revealed in this study will facilitate further identification of factors and mechanisms used in TLR signaling pathways.

Materials and Methods

Sample Preparation. The portion of the human MyD88 gene encoding the TIR domain (amino acid residues 148–296) was cloned into the vector pGEX-5X-3 (GE Healthcare). This vector was transformed into *Escherichia coli* BL-21 (DE3) (Novagen). The TIR domain of MyD88, which was expressed as a GST (GST) fusion protein, was first purified by glutathione Sepharose 4B FF (GE Healthcare) affinity chromatography, and the GST-tag was removed by digestion with Factor Xa (GE Healthcare). Subsequently, the TIR domain was purified by gel filtration (Sephacryl S-100 HR 26/60 column; GE Healthcare) and cation-exchange chromatography (Mono-S column; GE Healthcare). Using the purification protocol, ^{15}N-labeled, and ^{13}C, ^{15}N-doubly-labeled monomeric TIR domain of MyD88 wild-type proteins were prepared. The protein sample buffer was replaced by 20 mM potassium phosphate buffer (pH 6.0) containing 0.1 mM EDTA and 10 mM DTT. The final protein sample concentration for typical NMR experiments was approximately 0.3 mM.

NMR Spectroscopy. All NMR spectra were recorded at 25 °C on a Bruker DRX500 or DRX800 spectrometer equipped with a cryogenic probe. For assignment of backbone and side chain ^{1}H, ^{13}C, and ^{15}N resonances, a series of triple-resonance experiments were conducted (31). Distance restraints for structure calculations were obtained from 3D ^{15}N-edited NOESY and 3D ^{13}C-edited NOESY experiments, with a mixing time of 150 msec. NMR spectra were processed with NMRPipe software (32) and analyzed using Sparky (33). The pulse sequence used to obtain 2D {^{1}H}-^{15}N steady-state NOE spectra has been previously described (34). The {^{1}H}-^{15}N NOE values were determined from ratios of peak intensities with or without a 3 sec ^{1}H-saturation applied before each scan: NOE = I_{sat}/I_{unsat}.

Structure Calculation. Automated NOESY cross-peak assignment and iterative structure calculation were performed using CYANA version 2.1 (35). The obtained assignment of NOESY cross-peaks was manually validated, and the final structure calculation was performed using CNS version 1.1 (36). Surface electrostatic potentials were calculated using MOLMOL 2K.2 (37).

Cell Culture. Human embryonic kidney (HEK) 293-hTLR4A-HA cells were purchased from Invivogen. These cells were cultured in Dulbecco's modified Eagle's medium (high glucose-containing DMEM, Invitrogen) supplemented with 10% heat-inactivated FBS (Sigma), penicillin (100 U/ml), and streptomycin (100 pg/ml). All cells were incubated at 37 °C in a humidified atmosphere of 5% CO_2.

Vector Preparations. A cDNA encoding the TIR domain (amino acid residues 148–296) that was tagged at the N terminus with a myc-epitope was cloned into

the plasmid vector pcDNA3.1+ (Invitrogen). Mutants of the MyD88 TIR domain were generated using the GeneEditor in vitro Site-Directed Mutagenesis System (Promega). Mutants of each of 25 charged polar amino acid residues (Asp, Glu, Arg, Lys, and His) substituted by alanine were generated. Mutants with poor expression were not included to avoid possible misinterpretation of the loss of dominant negative inhibitory effect. The MD2 construct was also cloned into pcDNA3.1+. A pGL3-Basic Vector (Promega) containing 4 kB binding sites, which was used in the NF-κB luciferase reporter assay, and a Renilla luciferase reporter vector used as an internal control in the assay were gifts from Drs. Sewon Ki and Tetsuro Kokubo (Yokohama City University, Yokohama, Japan).

NF-κB Reporter Gene Activity. 293-hTLR4A-HA cells were transfected with pcDNA3.1+ control vector or pcDNA3.1+ myc-MyD88 TIR domain (wild type or mutant), pcDNA3.1+ MD2, NF-κB luciferase reporter vector, and Renilla luciferase reporter vector, using Lipofectamine 2000 (Invitrogen) according to the manufacturer's instructions. After transfection, the cells were stimulated with LPS O127 (1.0 μg/ml, Sigma) and incubated for 6 hours. Luciferase reporter gene activity was analyzed using the Dual-Luciferase Reporter Assay System (Promega). The inhibitory effect of each TIR mutant expression was assessed in at least 3 independent experiments. The statistical significance of differences in luciferase activities between wild type and mutants in the NF-κB reporter assays was analyzed using Dunnett's multiple comparison test. Statistical significance was assumed to be $P < 0.05$.

GST Pull-Down Assay. The TIR domain of MyD88 wild type and mutants (R196A, R196C, R217A, R288A, and R196A-R288A) was purified as GST-fusion proteins. These expression vectors were generated by subcloning the pcDNA3.1+myc-tagged MyD88 TIR domain into pGEX 5X-1 (GE Healthcare). The DD+ID of MyD88 (amino acid residues 18–141) and TLR4-TIR were also purified as GST-fusion proteins. The GST-fusion proteins were purified by glutathione Sepharose 4B FF (GE Healthcare) affinity chromatography. The TIR domain of human Mal, as well as the DD of IRAK4, was purified using a modified previously reported method (22, 38). These purified proteins were incubated with Glutathione Sepharose 4B (GE Healthcare) for 3 hours. After 4 wash steps with wash buffer (20 mM potassium phosphate buffer (pH 6.0), 100 mM KCl, 0.1 mM EDTA, 10 mM DTT, and 0.5% Triton X-100), the resin was analyzed by SDS polyacrylamide gel electrophoresis and Coomassie Brilliant Blue staining.

NMR Titration. One 15-μl aliquot of 100 μM nonlabeled Mal-TIR was added to 150 μl of 20 μM ^{15}N-labeled MyD88-TIR or its alanine substituted mutants up to 1.5 molar equivalent of ^{15}N MyD88-TIR. At each titration point, 1D ^{1}H-{^{15}N} and 2D ^{1}H-^{15}N SOFAST-HMQC spectra were measured. Quantification of NMR signal attenuation in the titration experiments, and evaluation of apparent dissociation constant (K_d^{app}) for the interaction, are described in *SI Materials and Methods.*

Docking Studies Between MyD88 and Mal. Structure modeling of the TIR domain of Mal was performed using the MyD88-TIR structure as a template on molecular operating environment (MOE) software (39, 40). The docking simulation was performed on AutoDock without any specific restraints between the molecules as previously reported (24, 41, 42). (See detailed method of the docking study in *SI Materials and Methods.*)

ACKNOWLEDGMENTS. We thank Dr. T. Fukao, Dr. H. Kaneko, Dr. Y. Aoki, Dr. H. Morita, Dr. T. Tokumi, W. Souma, and K. Kasahara for their advice and technical help. We thank Dr. S. Ki and Dr. T. Kokubo for their kind gift of vector samples. This work was funded in part by the Research and Development Program for New Bio-industry Initiatives (2005–2009) of the Bio-oriented Technology Research Advancement Institution, Japan. This work was supported by Grants-in-Aid for Scientific Research and the National Project on Protein Structural and Functional Analyses from the Ministry of Education, Science and Culture of Japan. This work was supported by Health and Labour Science Research Grants for Research on Allergic Disease and Immunology from the Ministry of Health, Labour and Welfare.

1. Bonnert TP, et al. (1997) The cloning and characterization of human MyD88: A member of an IL-1 receptor related family. *FEBS Lett* 402:81–84.
2. Kawai T, Akira S (2007) Signaling to NF-kappaB by Toll-like receptors. *Trends Mol Med* 13:460–469.
3. Akira S, Uematsu S, Takeuchi O (2006) Pathogen recognition and innate immunity. *Cell* 124:783–801.
4. Horng T, Barton GM, Flavell RA, Medzhitov R (2002) The adaptor molecule TIRAP provides signalling specificity for Toll-like receptors. *Nature* 420:329–333.
5. O'Neill LA, Bowie AG (2007) The family of five: TIR-domain-containing adaptors in Toll-like receptor signalling. *Nat Rev Immunol* 7:353–364.
6. Kagan JC, Medzhitov R (2006) Phosphoinositide-mediated adaptor recruitment controls Toll-like receptor signaling. *Cell* 125:943–955.
7. Rowe DC, et al. (2006) The myristoylation of TRIF-related adaptor molecule is essential for Toll-like receptor 4 signal transduction. *Proc Natl Acad Sci USA* 103:6299–6304.
8. Xu Y, et al. (2000) Structural basis for signal transduction by the Toll/interleukin-1 receptor domains. *Nature* 408:111–115.
9. Khan JA, Brint EK, O'Neill LA, Tong L (2004) Crystal structure of the Toll/interleukin-1 receptor domain of human IL-1RAPL. *J Biol Chem* 279:31664–31670.
10. Nyman T, et al. (2008) The crystal structure of the human Toll-like receptor 10 cytoplasmic domain reveals a putative signalingd. *J Biol Chem* 283:11861–11865.
11. Li C, Zienkiewicz J, Hawiger J (2005) Interactive sites in the MyD88 Toll/interleukin (IL) 1 receptor domain responsible for coupling to the IL1beta signaling pathway. *J Biol Chem* 280:26152–26159.
12. Jiang Z, et al. (2006) Details of Toll-like receptor:adapter interaction revealed by germ-line mutagenesis. *Proc Natl Acad Sci USA* 103:10961–10966.
13. von Bernuth H, et al. (2008) Pyogenic bacterial infections in humans with MyD88 deficiency. *Science* 321:691–696.
14. Burns K, et al. (1998) MyD88, an adapter protein involved in interleukin-1 signaling. *J Biol Chem* 273:12203–12209.
15. Slack JL, et al. (2000) Identification of two major sites in the type I interleukin-1 receptor cytoplasmic region responsible for coupling to pro-inflammatory signaling pathways. *J Biol Chem* 275:4670–4678.
16. Poltorak A, et al. (1998) Defective LPS signaling in C3H/HeJ and C57BL/10ScCr mice: Mutations in Tlr4 gene. *Science* 282:2085–2088.
17. Adachi O, et al. (1998) Targeted disruption of the MyD88 gene results in loss of IL-1- and IL-18-mediated function. *Immunity* 9:143–150.
18. Shimazu R, et al. (1999) MD-2, a molecule that confers lipopolysaccharide responsiveness on Toll-like receptor 4. *J Exp Med* 189:1777–1782.
19. Kagan JC, et al. (2008) TRAM couples endocytosis of Toll-like receptor 4 to the induction of interferon-beta. *Nat Immunol* 9:361–368.
20. Lu J, Chen M, Dekoster GT, Cistola DP, Li E (2008) The RXRalpha C-terminus T462 is a NMR sensor for coactivator peptide binding. *Biochem Biophys Res Commun* 366:932–937.
21. Burns K, et al. (2003) Inhibition of interleukin 1 receptor/Toll-like receptor signaling through the alternatively spliced, short form of MyD88 is due to its failure to recruit IRAK-4. *J Exp Med* 197:263–268.
22. Dunne A, Ejdeback M, Ludidi PL, O'Neill LA, Gay NJ (2003) Structural complementarity of Toll/interleukin-1 receptor domains in Toll-like receptors and the adaptors Mal and MyD88. *J Biol Chem* 278:41443–41451.
23. Brown V, Brown RA, Ozinsky A, Hesselberth JR, Fields S (2006) Binding specificity of Toll-like receptor cytoplasmic domains. *Eur J Immunol* 36:742–753.
24. Kato Z, et al. (2008) Positioning of autoimmune TCR-Ob. 2F3 and TCR-Ob. 3D1 on the MBP85–99/HLA-DR2 complex. *Proc Natl Acad Sci USA* 105:15523–15528.
25. Khor CC, et al. (2007) A Mal functional variant is associated with protection against invasive pneumococcal disease, bacteremia, malaria and tuberculosis. *Nat Genet* 39:523–528.
26. Horng T, Barton GM, Medzhitov R (2001) TIRAP: An adapter molecule in the Toll signaling pathway. *Nat Immunol* 2:835–841.
27. Mansell A, Brint E, Gould JA, O'Neill LA, Hertzog PJ (2004) Mal interacts with tumor necrosis factor receptor-associated factor (TRAF)-6 to mediate NF-kappaB activation by toll-like receptor (TLR)-2 and TLR4. *J Biol Chem* 279:37227–37230.
28. Piao W, et al. (2008) Tyrosine phosphorylation of MyD88 adapter-like (Mal) is critical for signal transduction and blocked in endotoxin tolerance. *J Biol Chem* 283:3109–3119.
29. Nunez Miguel R, et al. (2007) A dimer of the Toll-like receptor 4 cytoplasmic domain provides a specific scaffold for the recruitment of signalling adaptor proteins. *PLoS ONE* 2:e788.
30. Monie TP, Moncrieffe MC, Gay NJ (2009) Structure and regulation of cytoplasmic adapter proteins involved in innate immune signaling. *Immunol Rev* 227:161–175.
31. John C, Wayne JF, Arthur GIP, Rance M, Nicholas JS (2007) *Protein NMR Spectroscopy: Principles And Practice* (Academic, San Diego), 2nd Ed.
32. Delaglio F, et al. (1995) NMRPipe: A multidimensional spectral processing system based on UNIX pipes. *J Biomol NMR* 6:277–293.
33. Goddard TD, Kneller DG (1999) SPARKY 3 (University of California, San Francisco).
34. Farrow NA, et al. (1994) Backbone dynamics of a free and a phosphopeptide-complexed Src homology-2 domain studied by N-15 Nmr relaxation. *Biochemistry* 33:5984–6003.
35. Guntert P (2004) Automated NMR structure calculation with CYANA. *Methods Mol Biol* 278:353–378.
36. Brunger AT, et al. (1998) Crystallography & NMR system: A new software suite for macromolecular structure determination. *Acta Crystallogr D* 54:905–921.
37. Koradi R, Billeter M, Wuthrich K (1996) MOLMOL: A program for display and analysis of macromolecular structures. *J Mol Graphics 14:51-* 55:29–32.
38. Lasker MV, Gajjar MM, Nair SK (2005) Cutting edge: Molecular structure of the IL-1R-associated kinase-4 death domain and its implications for TLR signaling. *J Immunol* 175:4175–4179.
39. Levitt M (1992) Accurate modeling of protein conformation by automatic segment matching. *J Mol Biol* 226:507–533.
40. Fechteler T, Dengler U, Schomburg D (1995) Prediction of protein three-dimensional structures in insertion and deletion regions: A procedure for searching data bases of representative protein fragments using geometric scoring criteria. *J Mol Biol* 253:114–131.
41. Stoddard BL, Koshland DE, Jr (1992) Prediction of the structure of a receptor-protein complex using a binary docking method. *Nature* 358:774–776.
42. Morris GM, Goodsell DS, Huey R, Olson AJ (1996) Distributed automated docking of flexible ligands to proteins: Parallel applications of AutoDock 2.4. *J Comput Aided Mol Des* 10:293–304.

Brief report

Detection of T lymphocytes with a second-site mutation in skin lesions of atypical X-linked severe combined immunodeficiency mimicking Omenn syndrome

Taizo Wada,[1] Masahiro Yasui,[2] Tomoko Toma,[1] Yuko Nakayama,[1] Mika Nishida,[1] Masaki Shimizu,[1] Michiko Okajima[1], Yoshihito Kasahara,[1] Shoichi Koizumi,[1] Masami Inoue,[2] Keisei Kawa,[2] and Akihiro Yachie[1]

[1]Department of Pediatrics, Graduate School of Medical Science, Kanazawa University, Kanazawa; and [2]Department of Hematology/Oncology, Osaka Medical Center and Research Institute for Maternal and Child Health, Osaka, Japan

X-linked severe combined immunodeficiency (XSCID) is caused by mutations of the common gamma chain (γc) and usually characterized by the absence of T and natural killer (NK) cells. Here, we report an atypical case of XSCID presenting with autologous T and NK cells and Omenn syndrome-like manifestations. The patient carried a splice-site mutation (IVS1+5G>A) that caused most of the mRNA to be incorrectly spliced but produced normally spliced transcript in lesser amount, leading to residual γc expression and development of T and NK cells. The skin biopsy specimen showed massive infiltration of revertant T cells. Those T cells were found to have a second-site mutation and result in complete restoration of correct splicing. These findings suggest that the clinical spectrum of XSCID is quite broad and includes atypical cases mimicking Omenn syndrome, and highlight the importance of revertant mosaicism as a possible cause for variable phenotypic expression. (Blood. 2008;112: 1872-1875)

Introduction

Omenn syndrome (OS) is a peculiar immunodeficiency characterized by erythroderma, lymphadenopathy, hepatosplenomegaly, eosinophilia, hypogammaglobulinemia, elevated serum IgE, and activated/oligoclonal T cells.[1,2] The genes responsible for OS include *RAG1*, *RAG2*, *Artemis*, *RMRP*, and *IL7RA*.[3-8] Clinical manifestations resembling OS were demonstrated in cases of severe combined immunodeficiency (SCID) with maternal T-cell engraftment and of atypical DiGeorge syndrome.[9,10] In addition, we have recently reported an X-linked SCID (XSCID) patient with massive skin infiltration of natural killer (NK) cells, resulting in OS-like manifestations.[11] Here, we describe another case of XSCID mimicking OS. The patient carried a splice site mutation that allowed development of peripheral T and NK cells, and showed revertant T-cell mosaicism caused by a second-site mutation predominately in the skin. Both of these findings may have contributed to his phenotypic variation of XSCID.

Methods

Patient

A 5-month-old Japanese boy from nonconsanguineous parents was hospitalized because of failure to thrive, protracted diarrhea, and hypoproteinemia. He developed generalized erythematous rash and alopecia at 1 month of age (Figure 1A,B), followed by persistent cough, fever, hepatosplenomegaly, and lymphadenopathy. Laboratory studies revealed leukocytosis (60.0×10^9/L) with eosinophilia, liver dysfunction, and a low level of serum immunoglobulin G (IgG; 0.17 g/L). Serum IgE levels were significantly elevated at 1300 kIU/L. Immunophenotypic analysis of lymphocytes showed an increased percentage of $CD3^+$ T cells (93.1%), the majority expressing the activation markers CD45RO and HLA-DR. The ratio of $CD4^+$ to $CD8^+$ T cells was 1.1. The patient's $CD20^+$ B and $CD56^+$ NK cells were detectable at 3.8% and 3.2%, restrictively. The level of soluble interleukin-2 receptor was markedly elevated at 10 895 kIU/L. He had a normal thymus shadow. A skin biopsy exhibited massive lymphocytic infiltration and mild spongiosis (Figure 1C,D). His maternal half-brother died of interstitial pneumonia at infancy.

Cellular and molecular studies

Cell isolation, fluorescence-activated cell sorting (FACS) analysis for the common gamma chain (γc) and T-cell receptor (TCR) repertoire, spectratyping, microsatellite analysis, and mutation analysis of γc were performed as described elsewhere.[11-15] The purity of the sorted $CD4^+$ T, $CD8^+$ T, $CD19^+$ B, and $CD56^+$ NK cells was 98.1%, 99.3%, 86.4%, and 98.3%, respectively. T-cell and B-cell lines from the patient were established by transformation with Herpes virus saimiri and Epstein-Barr virus, respectively. Approval for the study was obtained from the Human Research Committee of Kanazawa University Graduate School of Medical Science, and informed consent was obtained in accordance with the Declaration of Helsinki.

Results and discussion

The patient's clinical findings were reminiscent of OS. However, he showed neither mutation in the *RAG* genes (data not shown) nor severely restricted TCR repertoire (Figure 1E,F). Microsatellite analysis ruled out maternal T-cell engraftment (Figure 1G). Because of possible X-linked inheritance in this family and our previous experience,[11] we assessed γc expression. FACS analysis clearly demonstrated defective γc expression on his lymphocytes and lymphocyte subpopulations, leading to the diagnosis of XSCID (Figure 1H). The patient had a G to A substitution at the fifth nucleotide of intron 1 of the *IL2RG* (IVS1+5G>A) that was previously listed in the IL2RG database (http://research.nhgri.

Submitted April 2, 2008; accepted May 28, 2008. Prepublished online as *Blood* First Edition paper, June 16, 2008; DOI 10.1182/blood-2008-04-149708.

The publication costs of this article were defrayed in part by page charge payment. Therefore, and solely to indicate this fact, this article is hereby marked "advertisement" in accordance with 18 USC section 1734.

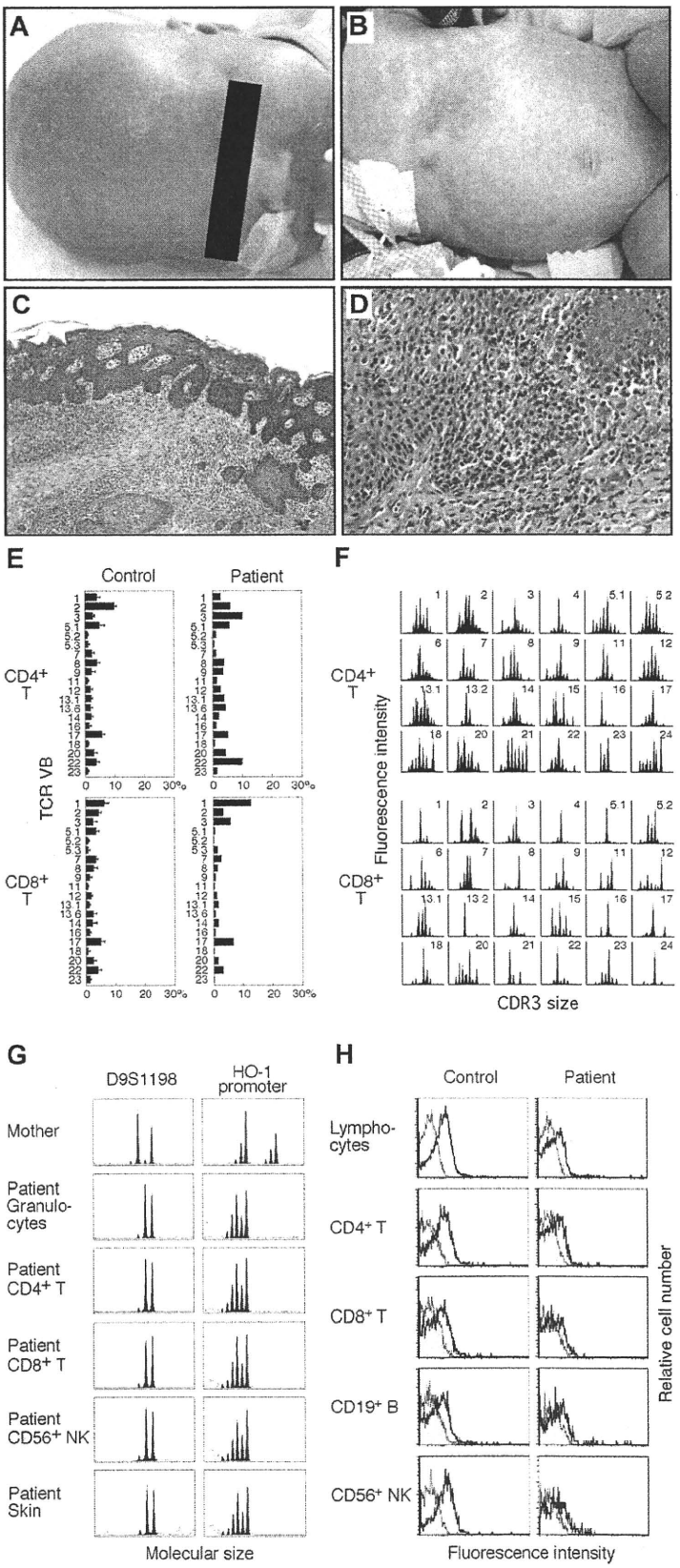

Figure 1. Skin lesions, skin biopsy specimen, T-cell receptor repertoire, microsatellite markers, and γc expression. (A) Alopecia. (B) Generalized scaling erythroderma. (C) Hematoxylin and eosin, original magnification ×40. (D) Hematoxylin and eosin, original magnification ×100. Micrographs were acquired using an Olympus BX51 microscope (Olympus, Melville, NY) fitted with 10× eyepieces, Olympus UPlanApo 4×/0.10 numeric aperture and 10×/0.40 numeric aperture objectives, a CoolSNAP cf CCD camera (Photometrics, Tucson, AZ), and Openlab image acquisition software version 3.1 (Improvision, Waltham, MA). Images were processed in Photoshop CS2 (Adobe Systems, San Jose, CA). (E) Expression profile of TCR variable β (VB) subfamilies. Peripheral blood samples were stained with monoclonal antibodies (mAbs) for individual TCR VB together with anti-CD4 and anti-CD8 mAbs. The percentage of each TCR VB expression within $CD4^+$ or $CD8^-$ T cells was analyzed by FACS. Error bars represent SD. (F) CDR3 spectratyping. Each TCR VB fragment was amplified from cDNA with one of the VB-specific primers. The size distribution of PCR products was determined by an automated sequencer and GeneScan software. (G) Microsatellite analysis. Two different markers were amplified with FAM-labeled specific primers and subjected to GeneScan analysis. HO-1 indicates heme oxygenase-1. (H) Analysis of γc expression on lymphocytes and lymphocyte subsets. Solid peaks indicate control Ab; open peaks represent anti-CD132 mAb.

nih.gov/apps/scid/IL2RGbase.shtml), and that caused most of the mRNA to be incorrectly spliced but produced, in lesser amount, normally spliced wild-type transcript (Figure 2A-D). When we analyzed such sequences in subcloned RT-PCR products obtained from his peripheral blood mononuclear cells, the wild-type sequence was detected in 15% of 20 clones. Accordingly, his

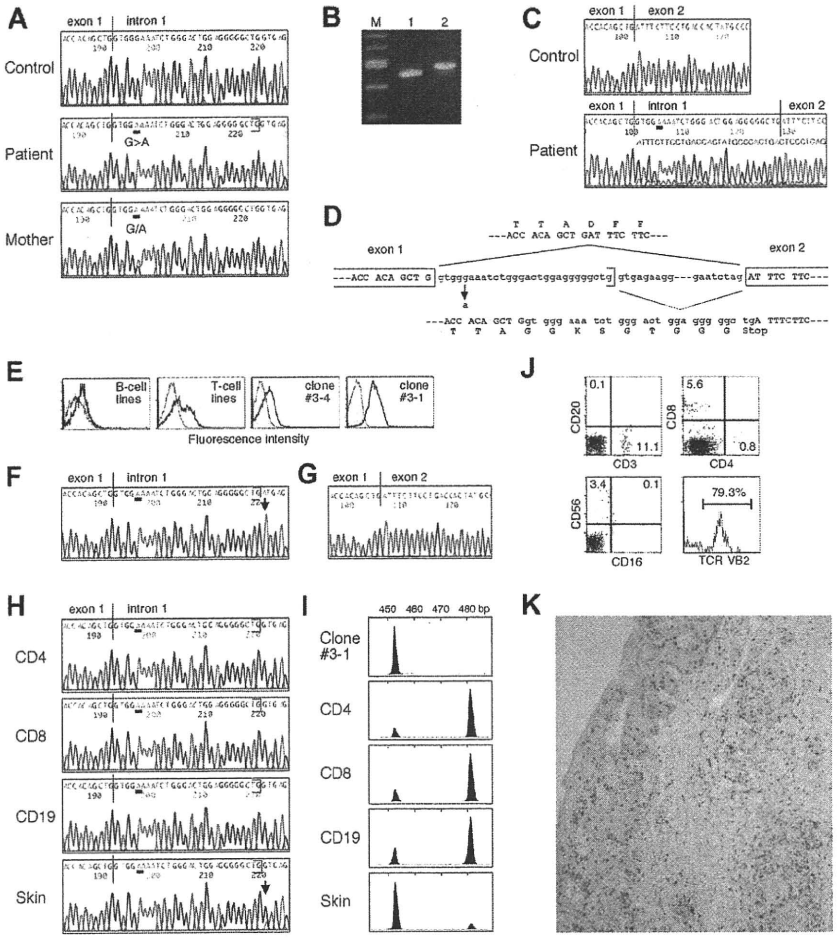

Figure 2. Characterization of inherited *IL2RG* gene mutation, second-site suppressor mutation, and skin-infiltrating lymphocytes. (A) The *IL2RG* gene was amplified from DNA extracted from normal, the patient's, and the mother's peripheral blood mononuclear cells (PBMCs). Direct sequence was performed using an automated sequencer. Bars show the locations of the mutation. (B) RT-PCR analysis for IL2RG mRNA using PBMCs obtained from normal control (lane 1) and the patient (lane 2). Lane M contains a 100-bp molecular size marker. (C) Direct sequence analysis of IL2RG cDNA using PBMCs from normal control and the patient. (D) Schematic representation of effect of the inherited splice-site mutation. (E) Analysis of γc expression. Shown are the results of γc expression on B-cell and T-cell lines, and cloned T cells #3-4 and #3-1 established from the patient. (F) Direct sequence analysis of *IL2RG* gene using DNA obtained from the clone #3-1. A bar shows the locations of the inherited mutation and an arrow highlights the second-site mutation. (G) Direct sequence analysis of IL2RG cDNA from the clone #3-1. (H) Direct sequencing analysis of *IL2RG* gene using DNA obtained from the patient's primary $CD4^+$ and $CD8^-$ T cells and $CD19^-$ B cells, and his skin. (I) GeneScan analysis of IL2RG cDNA amplified from the clone #3-1, the primary lymphocytes including $CD4^+$ and $CD8^-$ T cells and $CD19^-$ B cells, and the skin of the patient. A peak of the size of approximately 454 nucleotides represents wild-type mRNA and a second peak of approximately 482 nucleotides is generated by aberrant splicing. (J) FACS analysis of skin-infiltrating lymphocytes. The percentage of cells gated in each region is shown. (K) Immunohistochemical staining of the skin biopsy specimen. The samples were stained with anti-CD8 mAb.

lymphocytes showed the residual γc protein that likely permitted T- and NK-cell development to occur. Similar results were obtained from the study in another case of atypical XSCID with poorly functioning peripheral T cells.[16]

The presence of circulating T cells offered us a unique opportunity to establish T-cell lines from XSCID. Unexpectedly, FACS analysis showed a significant fraction of cells with normal γc expression among his T-cell lines (Figure 2E). Therefore, sequence analysis was performed using the cloned T-cell lines. We found the IVS1+5G>A in DNA from the γc-defective clone (#3-4), whereas DNA from the γc-expressing clone (#3-1) showed coexistence of the IVS1+5G>A and a second-site mutation (IVS1+29G>A), which was located at position +1 of the cryptic 5′ splice site (Figure 2F). Analysis of 100 normal chromosomes demonstrated the absence of the IVS1+5G>A and the IVS1+29G>A. The IVS1+29G>A was found to suppress the effect of the IVS1+5G>A and result in complete restoration of correct splicing that was consistent with the restored γc expression on the cell surface (Figure 2G). To determine whether the IVS1+29G>A was present in vivo, direct sequencing was performed with his various DNA samples. A peak of the IVS1+29G>A was only detectable in his skin specimen, but was absent among circulating $CD4^+$ and $CD8^+$ T and $CD19^+$ B cells (Figure 2H). When we analyzed the sequence in subcloned PCR products obtained from the skin, the IVS1+29G>A was detected in 12.9% of 31 clones. RT-PCR and GeneScan analysis demonstrated that a peak of the normal-sized transcript but not the mutated one was evident in the skin. Because IL2RG mRNA is expressed only in hematopoietic cells, these findings suggest that the majority of skin-infiltrating lymphocytes carry the IVS1+29G>A, thus indicating revertant cells (Figure 2I).

Although revertant γc expression would confer selective advantage in vivo to T- and NK-cell progenitors,[17] we could not detect the γc-expressing T cells in his circulation. This lack of in vivo selective advantage is in contrast to a previously described XSCID patient with revertant T-cell mosaicism in whom a reasonably diversified TCR repertoire was generated from a single T-cell progenitor, resulting in a mild clinical course.[18,19] The reasons underlying these findings are presently unclear. It is possible that the substantial numbers of activated peripheral T cells with defective γc expression that were not seen in the previous case[19] might have competed with the revertants, reduced the abilities of selective advantage of γc expression, and provided insufficient time for the reversion to reach the detection threshold in our patient. On the other hand, selective proliferation of revertant $CD8^-$ T cells with TCR VB2 in the skin (Figure 2J,K) may be due to a clonal expansion in response to infections or autoantigens and be involved in pathogenesis of his skin lesions. However, his complicated condition including the presence of autologous γc-defective T and NK cells in the peripheral blood and the expansion of revertant γc-expressing T cells in the skin does not allow us to draw clear conclusion about which aspects are responsible for the development of OS phenotype. Because recent studies in OS patients and murine models have indicated that impaired immune tolerance and

defective immune regulation play important roles in the pathophysiology of OS,[2,20] the highly elevated numbers of activated, γc-defective T cells with a moderate restricted TCR repertoire may have more contributed to the OS phenotype in our patient. If this is the case, it is possible that any SCID diseases having a profound but incomplete block in T-cell development could result in OS.

In summary, our studies indicate that the clinical spectrum of XSCID is broad and includes immunodeficient patients mimicking OS. In addition, the detection of the revertant T cells caused by the second-site suppressor mutation makes our case a second example of genetic reversion in XSCID and highlights the importance of somatic revertant mosaicism as a possible cause for atypical clinical presentations.

Acknowledgments

We thank Ms Harumi Matsukawa and Ms Emi Tamamura for excellent technical assistance.

This work was supported by a Grant-in-Aid for Scientific Research from the Ministry of Education, Culture, Sports, Science and Technology of Japan; and a grant from the Ministry of Health, Labour, and Welfare of Japan, Tokyo.

Authorship

Contribution: T.W. and A.Y. participated in designing and performing the research; T.T., Y.N., M.N., M.S., M.O., Y.K., and S.K. analyzed data; M.Y., M.I., and K.K. made clinical contributions and provided critical paper review; T.W. wrote the paper; and all authors checked the final version of the manuscript.

Conflict-of-interest disclosure: The authors declare no competing financial interests.

Correspondence: Taizo Wada, MD, PhD, Department of Pediatrics, Graduate School of Medical Science, Kanazawa University, 13-1 Takaramachi, Kanazawa 920-8641, Japan; e-mail: taizo@ped.m.kanazawa-u.ac.jp.

References

1. Omenn GS. Familial reticuloendotheliosis with eosinophilia. N Engl J Med. 1965;273:427-432.
2. Hönig M, Schwarz K. Omenn syndrome: a lack of tolerance on the background of deficient lymphocyte development and maturation. Curr Opin Rheumatol. 2006;18:383-388.
3. Villa A, Santagata S, Bozzi F, et al. Partial V(D)J recombination activity leads to Omenn syndrome. Cell. 1998;93:885-896.
4. Wada T, Toma T, Okamoto H, et al. Oligoclonal expansion of T lymphocytes with multiple second-site mutations leads to Omenn syndrome in a patient with RAG1-deficient severe combined immunodeficiency. Blood. 2005;106:2099-2101.
5. Dalal I, Tabori U, Bielorai B, et al. Evolution of a T-B-SCID into an Omenn syndrome phenotype following parainfluenza 3 virus infection. Clin Immunol. 2005;115:70-73.
6. Ege M, Ma Y, Manfras B, et al. Omenn syndrome due to ARTEMIS mutations. Blood. 2005;105:4179-4186.
7. Roifman CM, Gu Y, Cohen A. Mutations in the RNA component of RNase mitochondrial RNA processing might cause Omenn syndrome. J Allergy Clin Immunol. 2006;117:897-903.
8. Giliani S, Bonfim C, de Saint Basile G, et al. Omenn syndrome in an infant with IL7RA gene mutation. J Pediatr. 2006;148:272-274.
9. Müller SM, Ege M, Pottharst A, Schulz AS, Schwarz K, Friedrich W. Transplacentally acquired maternal T lymphocytes in severe combined immunodeficiency: a study of 121 patients. Blood. 2001;98:1847-1851.
10. Markert ML, Alexieff MJ, Li J, et al. Complete DiGeorge syndrome: development of rash, lymphadenopathy, and oligoclonal T cells in 5 cases. J Allergy Clin Immunol. 2004;113:734-741.
11. Shibata F, Toma T, Wada T, et al. Skin infiltration of $CD56^{bright}$ $CD16^{-}$ natural killer cells in a case of X-SCID with Omenn syndrome-like manifestations. Eur J Haematol. 2007;79:81-85.
12. Ariga T, Yamaguchi K, Yoshida J, et al. The role of common gamma chain in human monocytes in vivo; evaluation from the studies of X-linked severe combined immunodeficiency (X-SCID) carriers and X-SCID patients who underwent cord blood stem cell transplantation. Br J Haematol. 2002;118:858-863.
13. Puck JM, Pepper AE, Henthorn PS, et al. Mutation analysis of IL2RG in human X-linked severe combined immunodeficiency. Blood. 1997;89:1968-1977.
14. Tone Y, Wada T, Shibata F, et al. Somatic revertant mosaicism in a patient with leukocyte adhesion deficiency type 1. Blood. 2007;109:1182-1184.
15. Wada T, Konno A, Schurman SH, et al. Second-site mutation in the Wiskott-Aldrich syndrome (WAS) protein gene causes somatic mosaicism in two WAS siblings. J Clin Invest. 2003;111:1389-1397.
16. DiSanto JP, Rieux-Laucat F, Dautry-Varsat A, Fischer A, de Saint Basile G. Defective human interleukin 2 receptor gamma chain in an atypical X chromosome-linked severe combined immunodeficiency with peripheral T cells. Proc Natl Acad Sci U S A. 1994;91:9466-9470.
17. Cavazzana-Calvo M, Hacein-Bey S, de Saint Basile G, et al. Gene therapy of human severe combined immunodeficiency (SCID)-X1 disease. Science. 2000;288:669-672.
18. Bousso P, Wahn V, Douagi I, et al. Diversity, functionality, and stability of the T cell repertoire derived in vivo from a single human T cell precursor. Proc Natl Acad Sci U S A. 2000;97:274-278.
19. Stephan V, Wahn V, Le Deist F, et al. Atypical X-linked severe combined immunodeficiency due to possible spontaneous reversion of the genetic defect in T cells. N Engl J Med. 1996;335:1563-1567.
20. Marrella V, Poliani PL, Casati A, et al. A hypomorphic R229Q Rag2 mouse mutant recapitulates human Omenn syndrome. J Clin Invest. 2007;117:1260-1269.

ARTHRITIS & RHEUMATISM
Vol. 60, No. 1, January 2009, pp 242–250
DOI 10.1002/art.24134

Role of the *NOD2* Genotype in the Clinical Phenotype of Blau Syndrome and Early-Onset Sarcoidosis

Ikuo Okafuji,[1] Ryuta Nishikomori,[1] Nobuo Kanazawa,[2] Naotomo Kambe,[3] Akihiro Fujisawa,[1] Shin Yamazaki,[1] Megumu Saito,[1] Takakazu Yoshioka,[1] Tomoki Kawai,[1] Hidemasa Sakai,[1] Hideaki Tanizaki,[1] Toshio Heike,[1] Yoshiki Miyachi,[1] and Tatsutoshi Nakahata[1]

Objective. **Blau syndrome and its sporadic counterpart, early-onset sarcoidosis (EOS), share a phenotype featuring the symptom triad of skin rash, arthritis, and uveitis. This systemic inflammatory granulomatosis is associated with mutations in the *NOD2* gene. The aim of this study was to describe the clinical manifestations of Blau syndrome/EOS in Japanese patients and to determine whether the *NOD2* genotype and its associated basal NF-κB activity predict the Blau syndrome/EOS clinical phenotype.**

Methods. **Twenty Japanese patients with Blau syndrome/EOS and *NOD2* mutations were recruited. Mutated *NOD2* was categorized based on its basal NF-κB activity, which was defined as the ratio of NF-κB activity without a *NOD2* ligand, muramyldipeptide, to NF-κB activity with muramyldipeptide.**

Results. **All 9 mutations, including E383G, a novel mutation that was identified in 20 patients with Blau syndrome/EOS, were detected in the centrally located NOD region and were associated with ligand-independent NF-κB activation. The median age of the patients at disease onset was 14 months, although in 2 patients in Blau syndrome families (with mutations R334W and E383G, respectively) the age at onset was 5 years or older. Most patients with Blau syndrome/EOS had the triad of skin, joint, and ocular symptoms, the onset of which was in this order. Clinical manifestations varied even among familial cases and patients with the same mutations. There was no clear relationship between the clinical phenotype and basal NF-κB activity due to mutated *NOD2*. However, when attention was focused on the 2 most frequent mutations, R334W and R334Q, R334W tended to cause more obvious visual impairment.**

Conclusion. ***NOD2*** **genotyping may help predict disease progression in patients with Blau syndrome/EOS.**

Sarcoidosis is a systemic inflammatory disease with unknown etiology, but it can be clinically characterized by swelling of the bilateral hilar lymph nodes and histologically defined by the presence of noncaseating epithelioid cell granulomas. A special subtype called early-onset sarcoidosis (EOS; MIM no. 609464) occurs in children younger than 4 years of age and is characterized by a distinct triad of skin, joint, and eye disorders without apparent pulmonary involvement (1). An autosomal-dominant disease with clinical manifestations similar to those of EOS has been recognized as Blau syndrome (MIM no. 186580) (2,3). The gene responsible for Blau syndrome has been mapped close to the inflammatory bowel disease 1 (*IBD1*) locus by linkage analysis (4), and later the nucleotide-binding oligomerization domain 2 gene (*NOD2*) was identified by Miceli-Richard et al to be responsible for Blau syndrome (5). In the study by Miceli-Richard et al, 2 European patients with EOS had no mutation in *NOD2*; therefore, it remained

Supported by the Ministry of Education, Science, Sports, and Culture, Japan.

[1]Ikuo Okafuji, MD, Ryuta Nishikomori, MD, PhD, Akihiro Fujisawa, MD, PhD, Shin Yamazaki, PhD, Megumu Saito, MD, PhD, Takakazu Yoshioka, MD, Tomoki Kawai, MD, Hidemasa Sakai, MD, Hideaki Tanizaki, MD, Toshio Heike, MD, PhD, Yoshiki Miyachi, MD, PhD, Tatsutoshi Nakahata, MD, PhD: Kyoto University Graduate School of Medicine, Kyoto, Japan; [2]Nobuo Kanazawa, MD, PhD: Kyoto University Graduate School of Medicine, Kyoto, and Wakayama Medical University, Wakayama, Japan; [3]Naotomo Kambe, MD, PhD: Kyoto University Graduate School of Medicine, Kyoto, and Chiba University Graduate School of Medicine, Chiba, Japan.

Address correspondence and reprint requests to Ryuta Nishikomori, MD, PhD, Department of Pediatrics, Kyoto University Graduate School of Medicine, 54 Kawahara-cho, Shogoin, Sakyo-ku, Kyoto 606-8507, Japan. E-mail: rnishiko@kuhp.kyoto-u.ac.jp.

Submitted for publication March 19, 2008; accepted in revised form September 5, 2008.

controversial whether Blau syndrome and EOS have the same etiology.

In 2004, we encountered a 27-year-old Japanese man with multiple lichenoid papules. He was almost blind, exhibited camptodactyly, and had a continuous low-grade fever. This case of sporadic systemic granulomatosis with clinical features of EOS showed the same *NOD2* mutation, the arginine-to-tryptophan substitution at amino acid 334 (R334W), as that detected in Blau syndrome (6). Therefore, we expanded this report (6) and retrospectively examined cases of EOS in Japan and observed that 9 of 10 patients with EOS had *NOD2* mutations (7). Until recently, other investigators have also confirmed that Blau syndrome and EOS are clinically and genetically identical across various ethnic groups (8–10).

NOD2 activates NF-κB after recognizing a signal from a bacterial cell wall component, muramyldipeptide, in the cytoplasm of monocytes, and thus can work as an intracellular sensor of bacteria (11,12). *NOD2* has a tripartite domain structure consisting of 2 amino-terminal domains (termed caspase activation and recruitment domains) that are composed of protein–protein interaction cassettes, 1 centrally located NOD, and carboxy-terminal leucine-rich repeats (LRRs) (13). Using assays of NF-κB activity, an impaired ligand-dependent response was demonstrated for 3 Crohn's disease–associated mutations located in *NOD2* LRRs (14,15), whereas enhanced ligand-independent NF-κB activity was demonstrated for *NOD2* alleles associated with Blau syndrome and EOS (5,7,16). However, it remains unknown how increased basal NF-κB activity derived from gain-of-function mutations in *NOD2* affects the pathogenesis of Blau syndrome/EOS and whether a genotype–phenotype correlation exists between the clinical manifestations or onset of Blau syndrome/EOS and *NOD2* mutations.

Because Blau syndrome/EOS is so rare, very few reports are in the literature. Therefore, it was worthwhile to conduct a nationwide survey limited to patients with a specific ethnic background, such as Japanese patients. In this study, we precisely documented the clinical manifestations in a cohort of Japanese patients with Blau syndrome/EOS and *NOD2* mutations, including 9 previously reported cases (7), and explored the genotype–phenotype correlation to the basal NF-κB activity associated with each mutation, especially focusing on the correlation of visual impairment with the most frequent mutations, R334W and R334Q.

PATIENTS AND METHODS

Patients and clinical information. Among patients with clinically diagnosed Blau syndrome/EOS, the 20 patients with *NOD2* mutations were included in this study (7,17–20). None of these mutations were identical to the reported single-nucleotide polymorphisms (SNPs) of *NOD2*, nor were they detected in 100 Japanese healthy volunteers. Clinical information and patient histories were collected from medical records and by direct interviews of the patients and their attending physicians. The presence of each symptom was established as follows: a) persistent or repeated transient skin lesions without definite cause were determined, b) persistent or repeated transient arthritis without definite cause was determined, c) uveitis was diagnosed by an ophthalmologist, and d) remittent or intermittent fever without definite cause was determined under close examination at the time of hospital admission. The age at disease onset was defined as the age of the patient when any of the above-mentioned symptoms appeared.

Clinical evaluation was performed primarily when individual symptoms first appeared that were hardly affected by treatment or disease duration. The severity of visual impairment was assessed in accordance with the World Health Organization definition (21). Briefly, moderate visual impairment was defined as visual acuity between 6/18 and 3/60, and severe visual impairment was defined as acuity of 3/60 or less in the better eye with best correction, as previously described (9). Written informed consent was obtained from the patients and their families, and the study protocol was in accordance with the guidelines of the Institutional Review Board of Kyoto University Hospital.

Genetics analysis. Genomic DNA was extracted from the peripheral blood of the patients, and sequencing of all exons and exon–intron junctions of *NOD2* was performed as previously described (7).

Generation of *NOD2* mutants and NF-κB luciferase assay. Expression plasmids of *NOD2* and its mutants were subcloned into the p3xFLAG-CMV vector, as previously described (7). Blau syndrome/EOS–associated mutants were generated using the QuikChange site-directed mutagenesis kit (Stratagene, La Jolla, CA), as described previously (7). The ability of each construct to induce NF-κB activity was assessed by dual luciferase reporter assay in HEK 293 human embryonic kidney cells, as previously described (7).

Other analyses. We determined the age at the time of this survey, the age at onset of each symptom, and the *NOD2* genotype for all patients as well as the distribution of age at disease onset. Next, we analyzed the relationship between age at disease/symptom onset and basal NF-κB activity due to mutated *NOD2*. Basal NF-κB activity was defined as the ratio of NF-κB reporter activity without muramyldipeptide to NF-κB reporter activity with muramyldipeptide, as determined using the in vitro NF-κB luciferase assay described above. The activity was arbitrarily categorized as low (<0.3), moderate (0.3–0.5), and high (>0.5). Finally, we analyzed the relationship between visual impairment (normal, moderate, severe) and basal NF-κB activity (low, moderate, high) due to individual mutated *NOD2* genes, particularly the 2 most frequent mutations, R334W and R334Q. We did not perform statistical analysis because of the limited number of patients.

Table 1. Demographic and clinical characteristics of the patients with Blau syndrome/early-onset sarcoidosis*

Patient/ age/sex	Genotype	Fever		Skin rash		Arthritis		Uveitis		Visual acuity		Ref.
		Age at onset	Type	Age at onset	Type	Age at onset	Type	Age at onset	Type	OD	OS	
1/15/F†	E383G	2 yr 3 mo	Int	8 mo	LP/SE/EN	3 yr	Poly	11 yr	A/P	20/50	20/67	
2/48/F†	E383G	5 yr	Per	5 yr	LP/SE/EN	11 yr	Poly	11 yr	A/P	HM	Null	
3/36/F	H496L	–	–	1 yr	LP/SE	3 yr	Poly	5 yr	A/P	20/20	20/20	7
4/16/M	R334Q	1 yr 8 mo	Int	6 mo	LP/SE	1 yr 8 mo	Poly	1 yr 10 mo	A/P	20/22	20/22	
5/19/M	R334Q	2 yr 7 mo	Per	1 yr 4 mo	LP/SE/EN	10 mo	Poly	5 yr	A/P	20/50	20/20	17
6/8/F	R334Q	–	–	–	–	3 yr	Poly	–	–	20/20	20/20	
7/8/M	T605P	–	–	7 mo	LP/SE	1 yr 6 mo	Poly	3 yr 3 mo	A/P	20/25	20/50	7
8/18/F	D382E	–	–	3 yr 4 mo	LP/SE	4 yr	Poly	5 yr 4 mo	A/P	20/20	20/25	7, 18
9/13/M	R334W	8 mo	Per	1 yr 3 mo	LP/SE/EN	8 mo	Poly	1 yr 8 mo	A/P	20/29	20/33	
10/32/M	R334W	2 yr	Int	2 yr	LP/SE	1 yr 3 mo	Poly	6 yr	A/P	Blind, 20 yr	Blind, 20 yr	6, 7
11/21/F	R334W	2 yr 1 mo	Per	2 yr 1 mo	LP/SE	6 yr	Poly	4 yr	A/P	20/670	20/330	7, 19
12/33/M	R334W	–	–	2 yr	LP/SE	–	–	13 yr	A/P	20/29	20/20	7
13/31/F	R334W	–	–	2 yr 6 mo	LP/SE	8 yr	Poly	3 yr 6 mo	A/P	20/100	20/200	7
14/10/F†	R334W	1 yr	Per	1 yr	LP/SE	1 yr	Poly	2 yr	A/P	20/40	Null	
15/46/F†	R334W	–	–	44 yr	LP/SE	8 yr	Poly	3 yr	A/P	Blind, 28 yr	Blind, 28 yr	
16/16/M†	R334W	–	–	6 yr	SE	1 yr	Oligo	6 yr	A/P	20/13	20/13	20
17/18/F†	R334W	–	–	12 yr	SE	8 yr	Oligo	12 yr	A/P	20/40	20/25	20
18/8/M	M513T	2 yr 10 mo	Int	2 yr 8 mo	SE	2 yr 9 mo	Poly	2 yr 11 mo	A	20/17	20/17	7
19/15/F	N670K	1 yr 8 mo	Int	5 mo	LP/SE/EN	1 yr 8 mo	Poly	3 yr	A/P	20/200	20/200	7
20/7/M	C495Y	1 yr	Int	1 yr	LP/SE	1 yr	Poly	–		20/20	20/20	

* Patient 5 also had left ventricular dysfunction and pulmonary hemorrhage due to bronchial granuloma. Patient 10 also had interstitial pneumonia. Patient 11 also had hepatosplenomegaly and parotid swelling. Patient 18 also had renal calcification. OD = right eye; OS = left eye; yr = years; mo = months; Int = intermittent; LP = multiple lichenoid papules; SE = scaly erythematous plaques; EN = erythema nodosum–like lesion; Poly = polyarticular; A = anterior; P = posterior; Per = persistent; HM = hand motion; Oligo = oligoarticular.
† Familial case.

RESULTS

Genotype and basal NF-κB activity. The study population comprised 9 male patients and 11 female patients, with a median age of 17 years (range 7–48 years) and a median disease duration of 15 years (range 5–43 years). Fourteen of these 20 cases were sporadic (EOS), and 6 were familial (Blau syndrome). The familial cases were in 3 unrelated families; 2 families (patients 14 and 15 and patients 16 and 17, respectively) had Blau syndrome/EOS symptoms in 2 generations, and 1 family (patients 1 and 2) had Blau syndrome/EOS symptoms in 3 generations. The most frequent heterozygous mutation of *NOD2* was R334W (1000C>T), which was recognized in 2 familial and 5 sporadic cases (total of 9 cases), followed by R334Q (1001G>A) in 3 sporadic cases, and E383G (1148A>G, a novel amino acid substitution) in 2 familial cases (in 1 family). H496L (1487A>T), T605P (1813A>C), D382E (1146C>G), M513T (1538T>C), N670K (2010C>A), and C495Y (1484G>A) were detected in 1 sporadic case each (Table 1).

Nine mutations were identified in the centrally located NOD region (Figure 1a) and were associated with increased basal NF-κB activity in the absence of muramyldipeptide (Figure 1b), which is consistent with the finding of a previous study on Blau syndrome/EOS–associated *NOD2* mutations (16). We also confirmed that 100 healthy control subjects and their genotyped asymptomatic relatives did not have these amino acid substitutions. Therefore, we concluded that these *NOD2* mutations (amino acid substitutions) detected in patients with Blau syndrome/EOS were not SNPs but rather were disease-causing mutations.

Disease onset. The defining characteristic of EOS is its onset in children younger than age 4 years (1). In the present study, despite the median age at disease onset of 14 months, the first clinical symptoms developed at age 5 years or older in 2 patients (patients 2 and 17, who were members of different Blau syndrome families) with the E383G mutation and the R334W mutation, respectively (Table 2). In patient 2, skin rash developed at age 5 years; in patient 17, arthritis developed at age 8 years (Table 1).

The earliest presenting symptom was skin rash in 13 patients (65%), arthritis in 8 patients (40%), and ocular symptoms in 1 patient (patient 15, who had familial Blau syndrome with the R334W mutation) (Table 1). Approximately 95%, 95%, and 90% of pa-

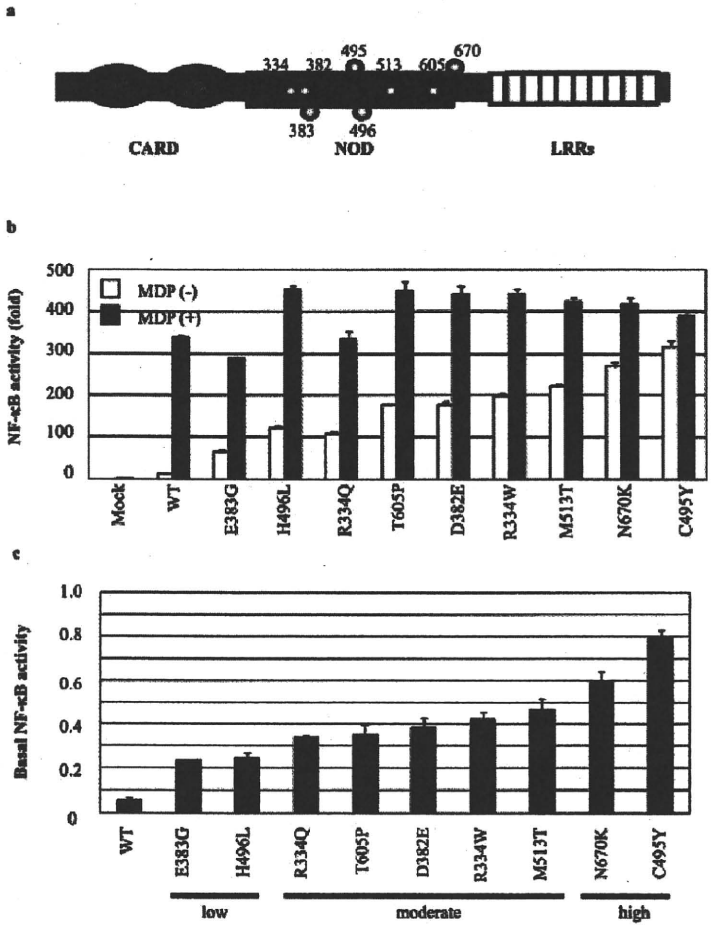

Figure 1. Biologic effects of *NOD2* mutants discovered in patients with Blau syndrome/early-onset sarcoidosis (EOS). **a,** Schematic presentation of NOD-2 protein. Numbers indicate the positions of mutated amino acid residues identified in our cohort. **b,** Increased basal NF-κB activity due to different mutated *NOD2* genes in patients with Blau syndrome/EOS. HEK 293T cells were cotransfected with a *NOD2* mutant together with the NF-κB reporter plasmid and internal control plasmid, and NF-κB reporter activity was measured after 12 hours of incubation with or without muramyldipeptide (MDP; 5 μg/ml). Mock vector and wild-type (WT) *NOD2* were used as controls. Bars show the mean and SD of normalized data (mock without muramyldipeptide = 1) from triplicate cultures. Results are representative of 3 independent experiments. **c,** Basal NF-κB activity due to mutated *NOD2* in patients with Blau syndrome/EOS. Bars show the mean and SD results from 3 independent experiments. CARD = caspase activation and recruitment domain; LRRs = leucine-rich repeats.

tients, respectively, had skin, joint, and ocular symptoms. Consistent with the previous report (1), a triad of skin, joint, and ocular symptoms developed (in this order) in many patients with Blau syndrome/EOS. The median age at onset of rash, arthritis, and uveitis was 24 months, 33 months, and 4.5 years, respectively (Table 2).

The triad of symptoms. All except 1 patient (patient 6 [with the R334Q mutation]) had skin manifestations. Consistent with a previous report (22), the most frequent skin symptom was scaly erythematous plaques with multiple lichenoid papules. Several patients (patients 1 and 2 with the E383G mutation, patient 5

Table 2. Age of the patients at the onset of disease and symptoms*

Age, years	Disease onset (n = 20)	Symptom onset			
		Fever (n = 11)	Rash (n = 19)	Arthritis (n = 19)	Uveitis (n = 18)
0	6 (30)	1 (9)	4 (21)	2 (11)	0 (0)
1	5 (25)	4 (36)	5 (26)	7 (37)	2 (11)
2	4 (20)	5 (45)	5 (26)	1 (5)	2 (11)
3	3 (15)	0 (0)	1 (5)	3 (16)	4 (22)
4	0 (0)	0 (0)	0 (0)	1 (5)	1 (6)
≥5	2 (10)	1 (9)	4 (21)	5 (26)	8 (44)

* Values are the number (%). The median age at disease onset was 1 year 2 months; the median age at onset of fever and rash was 2 years; the median age at onset of arthritis was 2 years 9 months; the median age at onset of uveitis was 4 years 6 months.

with the R334Q mutation, patient 9 with the R334W mutation, and patient 19 with the N670K mutation) had erythema nodosum–like lesions on their lower limbs in addition to solid lichenoid eruptions. Notably, 3 patients (patients 16 and 17 with the R334W mutation and patient 18 with the M513T mutation) showed only scaly erythematous plaques without lichenoid papules (Table 1).

All except 1 patient (patient 12 with the R334W mutation) had joint lesions (polyarticular arthritis in 17 patients and oligoarticular arthritis in 2 [patients 16 and 17]) (Table 1). Both patients with oligoarticular arthritis, who had familial Blau syndrome with the R334W mutation, had camptodactyly without obvious synovial cysts. Camptodactyly with synovial cysts is frequently described as a typical joint sign in patients with Blau syndrome/EOS (10). A consequence of arthritis was the use of a wheelchair for daily mobility in 2 patients (patient 5 with the R334Q mutation and patient 10 with the R334W mutation).

All except 2 patients (patient 6 with the R334Q mutation who also lacked skin eruptions and patient 20 with the C495Y mutation) had ocular lesions. The lesions were bilateral, although visual acuity was asymmetric, as in previous studies (22,23). Moreover, 17 (89%) of all 18 patients with ocular lesions had panuveitis, while only 1 patient (patient 18 with mutation M513T) had anterior uveitis, which demonstrated the predominance of panuveitis over anterior uveitis. Ocular symptoms were the last of the triad to develop in 15 of the 18 patients and the first to develop in only 1 patient (patient 15 with mutation R334W).

Clinical features other than the triad of symptoms. It is noteworthy that 11 patients (55%) experienced fever at a median age of 24 months, almost simultaneously with skin and/or joint symptoms (Table 1). Five patients had persistent fever reaching 38–40°C, and 6 patients had intermittent fever. In particular, in 1 patient (patient 9 with mutation R334W) the disease developed with intermittent fever (which then became persistent fever over the next 6 months) and finger joint swelling. In only 1 previous report (10), fever is mentioned as a clinical symptom of Blau syndrome/EOS, although there are some case reports in which fever was present at disease onset (24).

Four patients had involvement of organs other than the skin, joints, and eyes (Table 1). Two patients had pulmonary lesions (interstitial pneumonitis in patient 10 with the R334W mutation and bronchial granuloma in patient 5 with the R334Q mutation). Bilateral hilar lymph nodes, which are identified by chest radiography and/or computed tomographic scanning, were not observed in any patient. Patient 11 with the R334W mutation exhibited hepatosplenomegaly and parotid swelling (19), and patient 18 with the M513T mutation exhibited renal calcification. No cases of large-vessel vasculitis were observed in this cohort, even though vasculitis has been reported in patients with EOS (25–27).

Triggering factors. BCG vaccination was associated with the onset of disease (i.e., development of multiple papules on the extremities) in 2 patients, although no apparent infection or vaccination was clearly documented in other patients of our cohort. In 1 patient (patient 7 with mutation T605P) who had papules on the extremities, the spread of papules was from the site of BCG vaccination. In the other patient (patient 1 with mutation E383G), Gianotti disease was initially diagnosed, but a close review of her medical history later indicated that her multiple papules were a symptom of Blau syndrome/EOS.

Relationship between the onset of disease/symptoms and basal NF-κB activity due to mutated *NOD2*. Because disease duration and treatment varied among patients, we focused on the onset of disease and of each clinical symptom (i.e., fever, rash, arthritis, and uveitis). We evaluated the relationship between age at the onset of disease/symptoms and basal NF-κB activity due to mutated *NOD2* (defined as the ratio of NF-κB activity without a *NOD2* ligand, muramyldipeptide, to NF-κB activity with muramyldipeptide for each mutated *NOD2*). The calculated basal NF-κB activity ranged from 0.23 to 0.79 (mean 0.42) for mutated *NOD2* and was 0.05 for wild-type *NOD2* (Figure 1c).

Because the number of patients with each *NOD2* mutation was limited, we arbitrarily categorized basal NF-κB activity as low (<0.3), moderate (0.3–0.5), and high (>0.5). According to these criteria, mutations E383G and H496L were associated with low activity; mutations R334Q, T605P, D382E, R334W, and M513T were associated with moderate activity; and mutations

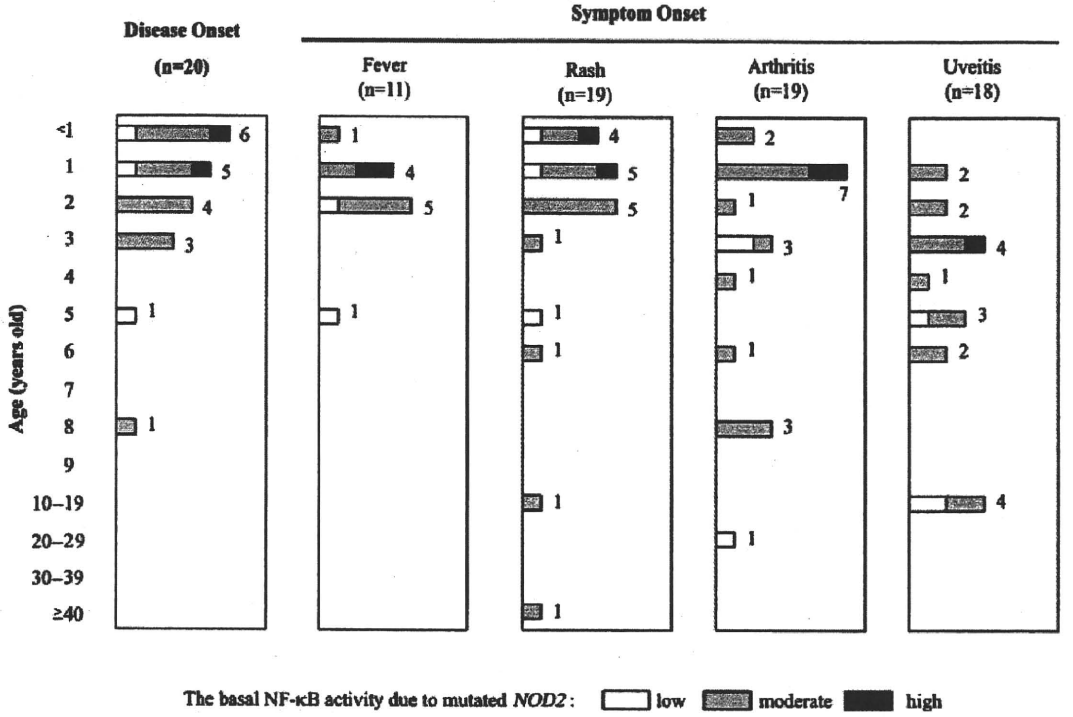

Figure 2. Relationship between age at disease or symptom onset and basal NF-κB activity due to mutated *NOD2*. Among the 9 patients without fever, 8 had moderate and 1 had low basal NF-κB activity. One patient without rash had moderate basal NF-κB activity, and 1 patient without arthritis had moderate basal NF-κB activity. Of 2 patients without uveitis, 1 had high and the other had moderate basal NF-κB activity.

N670K and C495Y were associated with high basal NF-κB activity. Our limited number of patients was insufficient to detect a correlation between the defined basal NF-κB activity and the onset of disease, fever, rash, arthritis, and uveitis (Figure 2). Notably, the age at onset of symptoms varied markedly between patients with the same R334W mutation, even in familial cases (Table 1).

Relationship between visual impairment and basal NF-κB activity due to mutated *NOD2*. The most relevant morbidity associated with Blau syndrome/EOS is ocular involvement, which is usually refractory to conventional treatment. Thus, we next explored the relationship between visual impairment and basal NF-κB activity. There was no clear correlation when the analysis included all recruited patients (Table 3). When we focused on the most frequent genotypes R334Q and R334W, between-genotype differences in visual impairment were observed (Table 4). Basal NF-κB activity was higher in patients with the R334W mutation than in those with the R334Q mutation (Figure 1c). None of the 3 patients with the R334Q mutation had visual impairments, while 4 of 9 patients with the R334W mutation

Table 3. Correlation between visual impairment and basal NF-κB activity*

	Visual impairment			Disease duration, median (range) years
	Normal	Moderate	Severe	
Basal NF-κB activity				
Low	2	0	1	35 (15–43)
Moderate	11	2	2	15 (5–43)
High	1	1	0	10.5 (6–15)

* Except where indicated otherwise, values are the number of patients.

Table 4. Correlation between visual impairment and the 2 most frequent genotypes*

	Visual impairment			Disease duration, median (range) years
	Normal	Moderate	Severe	
Present study				
R334Q	3	0	0	15 (5–19)
R334W	5	2	2	19 (9–43)
Previous study (9)				
R334Q	8	0	0	12 (3–26)
R334W	8	2	1	16 (5–44)

* Except where indicated otherwise, values are the number of patients.

had visual impairments. This result suggests that patients with the R334W mutation were more likely to have visual impairments than were those with the R334Q mutation (Table 4).

DISCUSSION

Blau syndrome/EOS is a rare systemic granulomatosis that has been associated with *NOD2*. In this study, patients with Blau syndrome/EOS and *NOD2* mutations were retrospectively recruited nationwide in Japan, to determine whether the *NOD2* genotype and its functional abnormality predict the Blau syndrome/EOS clinical phenotype. This study is the first to investigate the correlation between the *NOD2* genotype and its functional abnormality and the Blau syndrome/EOS clinical phenotype. Our findings suggest that *NOD2* genotyping may help predict disease progression in patients with Blau syndrome/EOS, although the clinical severity of Blau syndrome/EOS was not clearly associated with basal NF-κB activity due to mutated *NOD2* among the limited number of patients we studied.

The classic Blau syndrome/EOS symptom triad is skin rash, arthritis, and uveitis. Corresponding clinical manifestations include widespread erythematous papules, polyarthritis with boggy synovial swellings, and panuveitis (1,9,10,23), which were also identified in the present study. Rose et al described 2 patients who also had 1 episode of erythema nodosum–like lesions during the course of the disease (9). In our cohort, 5 patients had erythema nodosum–like lesions, suggesting that this should be recognized as one of the skin manifestations associated with Blau syndrome/EOS.

In the current study, 55% of the patients had fever, which always accompanied at least 1 symptom of the classic triad. Arostegui et al also reported that 50% of their cohort had recurrent or persistent fever (10). These findings suggest that fever is one of the important symptoms of Blau syndrome/EOS and is the reason why Blau syndrome/EOS is misdiagnosed as systemic-onset juvenile idiopathic arthritis (JIA). In fact, patient 11 in our study (who had the R334W mutation) experienced persistent fever reaching 40°C and received aggressive immunosuppressive therapy, because systemic-onset JIA was initially diagnosed. This case alerts us to the possibility that patients with Blau syndrome/EOS can sometimes have fever, and that Blau syndrome/EOS can resemble systemic-onset JIA.

Bilateral hilar lymph nodes, which are often seen in adult sarcoidosis, are not observed in Blau syndrome/EOS, but this does not mean that pulmonary lesions do not occur in patients with Blau syndrome/EOS. In fact, 2 patients (patient 5 [with the R334Q mutation] and patient 10 [with the R334W mutation]) had pulmonary lesions; in particular, patient 10 had the first reported case of sporadic EOS in association with the *NOD2* mutation (6). Another case of Blau syndrome/EOS with pulmonary lesions and interstitial pneumonitis, but not bilateral hilar lymph nodes, has also been reported (28). These findings suggest the importance of following up patients with Blau syndrome/EOS to check for not only the classic triad of symptoms but also other abnormalities, including pulmonary lesions.

Blau syndrome/EOS, which usually occurs in children younger than age 4 years, developed at 5 years and 8 years, respectively, in 2 patients in the present study (patient 2 [with the E383G mutation] and patient 17 [with the R334W mutation]). Because both of these patients had a family history of skin rash/arthritis/uveitis, they had been closely monitored by their parents as well as by their physicians. Therefore, it is unlikely that any symptoms that occurred when the patients were younger than 4 years of age were overlooked in these 2 cases. In the literature, there is 1 case of Blau syndrome in which skin rash, persistent fever, and camptodactyly started to develop at age 18 years (10). These findings indicate that the onset of Blau syndrome/EOS can be at age 5 years or older, and that disease onset in a patient younger than 4 years should not be considered requisite for a diagnosis of Blau syndrome/EOS.

In our cohort, the age at disease/symptom onset, organ involvement, and severity of Blau syndrome/EOS varied substantially even within affected families and between individuals with the same *NOD2* mutation (e.g., R334W). In other genetic disorders, identical mutations have been associated with phenotypic variation in unrelated individuals, within a family, and even in monozygotic twins (29). Phenotypic variation in Blau syndrome/EOS has been reported in monozygotic twins; therefore, nongenetic factors such as environmental conditions and/or infectious agents might be involved in phenotypic variation (24). Interestingly, in 2 of our cases, BCG vaccination was an obvious triggering factor. In addition, a previous report noted that cutaneous lesions first arose after BCG vaccination in a patient with Blau syndrome/EOS (30). The BCG vaccine contains muramyldipeptide, a ligand for NOD-2 protein (11,12), which is interesting from a pathophysiologic point of view. However, BCG vaccination did not always cause the onset of disease in patients with Blau syndrome/EOS, because most patients in our cohort were vaccinated with BCG according to the immunization protocol used in areas of

Japan where the risk for tuberculosis was high. An unknown endogenous ligand for NOD-2 could influence disease onset and/or progression, similar to uric acid as an endogenous cryopyrin/NLRP3 ligand (31). The potential roles of endogenous ligands, pathogen-associated molecular patterns, and/or danger-associated molecular patterns in disease pathogenesis remain to be elucidated.

Although increased basal NF-κB activity due to mutated *NOD2* has been proposed as an etiology of Blau syndrome/EOS, how such activity causes the characteristic symptoms remains unclear. We hypothesized that if increased basal NF-κB activity is the key to the pathophysiology of this disease, it should be related to disease severity or disease progression. Unfortunately, there was no clear correlation between basal NF-κB activity and the onset of disease/symptoms. However, patients with mutated *NOD2* and low basal NF-κB activity tended to experience complications, e.g., arthritis and uveitis, at a later age. This finding raises the possibility that basal NF-κB activity may affect disease progression rather than disease onset. Given that NOD-2 protein signals through MAPK/ERK as well as the NF-κB pathway (32), the possibility cannot be excluded that the MAPK/ERK activation potential of each *NOD2* genotype might also be correlated with disease severity or progression.

From the perspective of quality of life, the ocular manifestations of Blau syndrome/EOS require the closest attention (33). In a previous study, one-third of patients with Blau syndrome/EOS and *NOD2* mutations had a poor or extremely poor visual outcome, and the progression of visual field loss was independent of the particular *NOD2* mutant and was not associated with disease duration (9). In our cohort, however, patients with the R334W mutation experienced more visual impairment than did patients with the R334Q mutation, although 4 patients with the R334W mutation were from 2 families (patients 14 and 15 and patients 16 and 17, respectively). Therefore, familial genetic and environmental factors could easily influence the phenotype. Thus, in order not to favor our hypothesis, we excluded patients 15 and 17 from the analysis, and the trend was still evident. This observation was consistent with the findings of Rose et al (9), although those investigators did not address this issue. These findings suggest that *NOD2* genotyping could help predict the course of eye disease in patients with Blau syndrome/EOS, especially those with the R334Q mutation or the R334W mutation.

The relationship between visual impairment and basal NF-κB activity also remains a matter for discussion. Our data showed that visual impairments were more severe in patients with the R334W mutation than in those with the R334Q mutation, which seems to be consistent with the hypothesis that higher basal NF-κB activity causes more severe disease or more disease progression. However, no ocular symptoms have developed during the 6 years since disease onset in patient 20 (with the C495Y mutation and the highest basal NF-κB activity in our cohort), although ocular symptoms developed in another patient with the same genotype (10). Also, in patient 2, who had the E383G mutation and the lowest basal NF-κB activity, severe visual impairment occurred when she was in her late twenties. These findings contradict our hypothesis that *NOD2* genotypes with higher basal NF-κB activity are associated with severe disease. However, Blau syndrome/EOS was promptly diagnosed in patient 20 with the C495Y mutation, who luckily was under the care of the same pediatric rheumatologist who treated patient 19 (who had the N670K mutation) and was treated with systemic steroid therapy. Patient 2 (who had the E383G mutation) subsequently received inappropriate immunosuppressive therapy, because the patient refused steroid treatment. Furthermore, patient 10 (with the R334W mutation), who had no obvious systemic inflammatory findings and did not receive systemic steroid therapy, became blind at 20 years of age. These findings raise the possibility that the extent of visual impairment could be modified by therapy.

Finally, we were not able to prove a link between the clinical severity of Blau syndrome/EOS and basal NF-κB activity in the whole cohort, possibly because of the restricted number of patients and because of the differences in treatment among patients. Therefore, a prospective study involving a sufficient number of patients to allow analysis of each genotype–phenotype correlation would be required to test our hypothesis. Given that there is no standard treatment protocol for Blau syndrome/EOS, some predictors of disease progression, especially progression of visual impairment, would have great benefit for clinicians. We observed a difference in the development of visual impairment only between patients with the R334W mutation and those with the R334Q mutation, which provides a clue that predicts the development of visual impairment in patients with the R334W and R334Q mutations. We also believe that understanding the mechanisms of how *NOD2* acts in disease pathogenesis should help in discovering therapeutic targets for the treatment of Blau syndrome/EOS.

ACKNOWLEDGMENTS

We appreciate the invaluable assistance of the following physicians, who kindly provided materials and allowed us to study their patients: Drs. Sonoko Nagai, Takenosuke Yuasa, Akira Manki, Yoshihiko Sakurai, Mitsuru Nakajima, Hiroko Kobayashi, Ikuma Fujiwara, Hiroyuki Tsutsumi, Shuji Takei, Kumiko Nakao, Yoshikazu Otsubo, Kouichi Ohta, Kazunaga Agematsu, Hiroaki Azukisawa, Hiroyuki Murota, and Kenji Katamura.

AUTHOR CONTRIBUTIONS

Dr. Nishikomori had full access to all of the data in the study and takes responsibility for the integrity of the data and the accuracy of the data analysis.

Study design. Okafuji, Nishikomori, Heike, Miyachi, Nakahata.
Acquisition of data. Okafuji, Fujisawa, Saito, Yoshioka, Kawai, Sakai, Tanizaki.
Analysis and interpretation of data. Okafuji, Nishikomori.
Manuscript preparation. Okafuji, Nishikomori, Kanazawa, Kambe.
Statistical analysis. Yamazaki.

REFERENCES

1. Hetherington S. Sarcoidosis in young children. Am J Dis Child 1982;136:13–5.
2. Blau EB. Familial granulomatous arthritis, iritis, and rash. J Pediatr 1985;107:689–93.
3. Jabs DA, Houk JL, Bias WB, Arnett FC. Familial granulomatous synovitis, uveitis, and cranial neuropathies. Am J Med 1985;78:801–4.
4. Ohmen JD, Yang HY, Yamamoto KK, Zhao HY, Ma Y, Bentley LG, et al. Susceptibility locus for inflammatory bowel disease on chromosome 16 has a role in Crohn's disease, but not in ulcerative colitis. Hum Mol Genet 1996;5:1679–83.
5. Miceli-Richard C, Lesage S, Rybojad M, Prieur AM, Manouvrier-Hanu S, Hafner R, et al. CARD15 mutations in Blau syndrome. Nat Genet 2001;29:19–20.
6. Kanazawa N, Matsushima S, Kambe N, Tachibana T, Nagai S, Miyachi Y. Presence of a sporadic case of systemic granulomatosis syndrome with a CARD15 mutation. J Invest Dermatol 2004;122: 851–2.
7. Kanazawa N, Okafuji I, Kambe N, Nishikomori R, Nakata-Hizume M, Nagai S, et al. Early-onset sarcoidosis and CARD15 mutations with constitutive nuclear factor-κB activation: common genetic etiology with Blau syndrome. Blood 2005;105:1195–7.
8. Rose CD, Doyle TM, McIlvain-Simpson G, Coffman JE, Rosenbaum JT, Davey MP, et al. Blau syndrome mutation of CARD15/NOD2 in sporadic early onset granulomatous arthritis. J Rheumatol 2005;32:373–5.
9. Rose CD, Wouters CH, Meiorin S, Doyle TM, Davey MP, Rosenbaum JT, et al. Pediatric granulomatous arthritis: an international registry. Arthritis Rheum 2006;54:3337–44.
10. Arostegui JI, Arnal C, Merino R, Modesto C, Carballo MA, Moreno P, et al. NOD2 gene–associated pediatric granulomatous arthritis: clinical diversity, novel and recurrent mutations, and evidence of clinical improvement with interleukin-1 blockade in a Spanish cohort. Arthritis Rheum 2007;56:3805–13.
11. Girardin SE, Boneca IG, Viala J, Chamaillard M, Labigne A, Thomas G, et al. Nod2 is a general sensor of peptidoglycan through muramyl dipeptide (MDP) detection. J Biol Chem 2003; 278:8869–72.
12. Inohara N, Ogura Y, Fontalba A, Gutierrez O, Pons F, Crespo J, et al. Host recognition of bacterial muramyl dipeptide mediated through NOD2: implications for Crohn's disease. J Biol Chem 2003;278:5509–12.
13. Ogura Y, Inohara N, Benito A, Chen FF, Yamaoka S, Nunez G. Nod2, a Nod1/Apaf-1 family member that is restricted to monocytes and activates NF-κB. J Biol Chem 2001;276:4812–8.
14. Hugot JP, Chamaillard M, Zouali H, Lesage S, Cezard JP, Belaiche J, et al. Association of NOD2 leucine-rich repeat variants with susceptibility to Crohn's disease. Nature 2001;411:599–603.
15. Ogura Y, Bonen DK, Inohara N, Nicolae DL, Chen FF, Ramos R, et al. A frameshift mutation in NOD2 associated with susceptibility to Crohn's disease. Nature 2001;411:603–6.
16. Chamaillard M, Philpott D, Girardin SE, Zouali H, Lesage S, Chareyre F, et al. Gene-environment interaction modulated by allelic heterogeneity in inflammatory diseases. Proc Natl Acad Sci U S A 2003;100:3455–60.
17. Yotsumoto S, Takahashi Y, Takei S, Shimada S, Miyata K, Kanzaki T. Early onset sarcoidosis masquerading as juvenile rheumatoid arthritis. J Am Acad Dermatol 2000;43(5 Pt 2):969–71.
18. Ukae S, Tsutsumi H, Adachi N, Takahashi H, Kato F, Chiba S. Preschool sarcoidosis manifesting as juvenile rheumatoid arthritis: a case report and a review of the literature of Japanese cases. Acta Paediatr Jpn 1994;36:515–8.
19. Sakurai Y, Nakajima M, Kamisue S, Nishimura Y, Ueda T, Miyagawa S, et al. Preschool sarcoidosis mimicking juvenile rheumatoid arthritis: the significance of gallium scintigraphy and skin biopsy in the differential diagnosis. Acta Paediatr Jpn 1997;39:74–8.
20. Kurokawa T, Kikuchi T, Ohta K, Imai H, Yoshimura N. Ocular manifestations in Blau syndrome associated with a CARD15/Nod2 mutation. Ophthalmology 2003;110:2040–4.
21. Resnikoff S, Pascolini D, Etya'ale D, Kocur I, Pararajasegaram R, Pokharel GP, et al. Global data on visual impairment in the year 2002. Bull World Health Organ 2004;82:844–51.
22. North AF Jr, Fink CW, Gibson WM, Levinson JE, Schuchter SL, Howard WK, et al. Sarcoid arthritis in children. Am J Med 1970;48:449–55.
23. Lindsley CB, Petty RE. Overview and report on international registry of sarcoid arthritis in childhood. Curr Rheumatol Rep 2000;2:343–8.
24. Milman N, Andersen CB, Hansen A, van Overeem Hansen T, Nielsen FC, Fledelius H, et al. Favourable effect of TNF-α inhibitor (infliximab) on Blau syndrome in monozygotic twins with a de novo CARD15 mutation. APMIS 2006;114:912–9.
25. Rotenstein D, Gibbas DL, Majmudar B, Chastain EA. Familial granulomatous arteritis with polyarthritis of juvenile onset. N Engl J Med 1982;306:86–90.
26. Gross KR, Malleson PN, Culham G, Lirenman DS, McCormick AQ, Petty RE. Vasculopathy with renal artery stenosis in a child with sarcoidosis. J Pediatr 1986;108:724–6.
27. Rose CD, Eichenfield AH, Goldsmith DP, Athreya BH. Early onset sarcoidosis with aortitis: "juvenile systemic granulomatosis?" [published erratum appears in J Rheumatol 1990;17:575]. J Rheumatol 1990;17:102–6.
28. Becker ML, Martin TM, Doyle TM, Rose CD. Interstitial pneumonitis in Blau syndrome with documented mutation in CARD15. Arthritis Rheum 2007;56:1292–4.
29. Wolf U. Identical mutations and phenotypic variation [review]. Hum Genet 1997;100:305–21.
30. Osborne GE, Mallon E, Mayou SC. Juvenile sarcoidosis after BCG vaccination. J Am Acad Dermatol 2003;48(5 Suppl):S99–102.
31. Martinon F, Petrilli V, Mayor A, Tardivel A, Tschopp J. Gout-associated uric acid crystals activate the NALP3 inflammasome. Nature 2006;440:237–41.
32. Pauleau AL, Murray PJ. Role of Nod2 in the response of macrophages to Toll-like receptor agonists. Mol Cell Biol 2003; 23:7531–9.
33. Fink CW, Cimaz R. Early onset sarcoidosis: not a benign disease. J Rheumatol 1997;24:174–7.